Horizon 2020
Programme

CORTEX

Research and Innovation Action (RIA)

This project has received funding from the European Union's Horizon 2020 research and innovation programme under grant agreement No 754316.

Start date : 2017-09-01 Duration : 48 Months
http://cortex-h2020.eu

Development and comparison of highorder solvers for reactor noise analysis

Authors : Mr. Paolo VINAI (Chalmers), Alberto BRIGHENTI (CEA), Christophe DEMAZIÈRE (Chalmers), Baptiste GASSE (CEA), Damián GINESTAR (UPV), Antonios MYLONAKIS (Chalmers), Amélie ROUCHON (CEA), Simone SANTANDREA (CEA), Andreas TATIDIS (Chalmers), Antoni VIDAL-FERRÀNDIZ (UPV), Gumersindo VERDÚ (UPV), Toshihiro YAMAMOTO (KyotoU), Huaiqian YI (Chalmers), Igor ZMIJAREVIC (CEA), Andrea ZOIA (CEA)

CORTEX - Contract Number: 754316

Project officer: Marco Carbini

Document title	Development and comparison of highorder solvers for reactor noise analysis
Author(s)	Mr. Paolo VINAI, Alberto BRIGHENTI (CEA), Christophe DEMAZIÈRE (Chalmers), Baptiste GASSE (CEA), Damián GINESTAR (UPV), Antonios MYLONAKIS (Chalmers), Amélie ROUCHON (CEA), Simone SANTANDREA (CEA), Andreas TATIDIS (Chalmers), Antoni VIDAL-FERRÀNDIZ (UPV), Gumersindo VERDÚ (UPV), Toshihiro YAMAMOTO (KyotoU), Huaiqian YI (Chalmers), Igor ZMIJAREVIC (CEA), Andrea ZOIA (CEA)
Number of pages	38
Document type	Deliverable
Work Package	WP01
Document number	D1.4
Issued by	Chalmers
Date of completion	2021-08-09 16:12:58
Dissemination level	Public

Summary

In the CORTEX project, solvers and procedures based on Monte Carlo and on deterministic higher-order transport methods are developed and compared for neutron noise simulations. These computational tools allow a more accurate modeling of the system response to small, stationary perturbations. Therefore, they produce more detailed simulations that can be used for a better understanding of neutron noise problems and for the investigation of limitations of less accurate approximations such as neutron diffusion theory.

Approval

Date	By
2021-08-09 16:15:02	Mr. Paolo VINAI (Chalmers)
2021-08-10 08:02:47	Pr. Christophe DEMAZIERE (Chalmers)

Table of Contents

Index of Tables

Table of Figures

This project has received funding from the Euratom research and training programme 2014-2018 under the grant agreement no.754316. The content in this report reflects only the views of the authors. The European Commission is not responsible for any use that may be made of the information it contains.

Abbreviations

adCMFD	Artificially Diffusive Coarse Mesh Finite Difference
APSD	Auto Power Spectral Density
CEA	The French Alternative Energies and Atomic Energy Commission
CMFD	Coarse Mesh Finite Difference
CORTEX	Core monitoring techniques and experimental validation and demonstration
CPSD	Cross Power Spectral Density
IDT	Integral-Differential Transport
IPK	Improved Point-Kinetics
KU	Kyoto University
MOSC	Method of Short Characteristics
TDT	Two/Three Dimensional Transport

Summary

In the CORTEX project, solvers and procedures based on Monte Carlo and on deterministic higher-order transport methods are developed and compared for neutron noise simulations. These computational tools allow a more accurate modeling of the system response to small, stationary perturbations. Therefore, they produce more detailed simulations that can be used for a better understanding of neutron noise problems and for the investigation of limitations of less accurate approximations such as neutron diffusion theory.

1 Introduction

During normal, steady-state operations of a nuclear reactor, neutron flux measurements are characterized by small fluctuations around mean values. These fluctuations are referred to as neutron noise, and they may be driven by a variety of perturbations, such as mechanical vibrations of core internals, disturbances in the coolant flow, etc.

In the CORTEX project [1], core monitoring and diagnostics techniques are developed to identify anomalous patterns in a nuclear reactor from the analysis of the neutron noise, so that appropriate actions can be taken at an early stage and prevent potentially dangerous situations from escalating. For this purpose, a crucial task is to model the reactor transfer function, which describes the core response to a possible perturbation. Knowing the reactor transfer function allows to retrieve information about the perturbations from the neutron flux measurements via an inversion algorithm, which can be based on advanced signal processing techniques or machine learning, see, e.g., [2-4].

The reactor transfer function is modelled using the neutron transport equation, while the possible perturbations are expressed in terms of changes in the macroscopic nuclear cross sections. As discussed in [5], a coarser estimation of the reactor transfer function may be sufficient for core monitoring and diagnostics, and most of the work in the field of reactor neutron noise relies on neutron diffusion theory, see, e.g., [6-7]. However, recent efforts also focused on the development of stochastic methods and higher-order deterministic methods to perform more detailed analyses and assess the limitations of the diffusion approximation for neutron noise applications.

Work on the modelling of the reactor transfer function using stochastic and higher-order deterministic methods has been carried out in task 1.3 of the CORTEX project and is reported in the current document. It includes the development, consolidation and study of different solvers and procedures, i.e., the discrete ordinates solver NOISE-SN (section 2), the frequency-domain APOLLO3® IDT solvers (section 3), the time-domain APOLLO3® IPK solver (section 4), a Monte Carlo-based procedure for neutron noise calculations (section 5), the frequency-domain solver in the stochastic code TRIPOLI-4® (section 6), and a stochastic neutron noise solver developed by Kyoto University (section 7). Results obtained from the comparison between these solvers and from the comparison with diffusion approximations are discussed in section 8. Conclusions are drawn in section 9.

2 NOISE-SN

The solver NOISE-SN is based on the transport neutron noise equation in the frequency domain. The discretization of the equations is performed according to a finite difference, discrete ordinates, multi-energy group method. The algorithm for the numerical solution is accelerated using the CMFD method. The solver allows to simulate 2-D and 3-D systems with reflective and vacuum boundary conditions. For the mitigation of possible ray effects in 2-D problems, the equations are modified with a fictitious source term. A detailed description of the solver and its application can be found, e.g., in [8-10].

2.1 Governing equations

In the case of a nuclear reactor, the multi-energy-group time-dependent neutron transport equation with a generic number of families of delayed-neutron precursors is written as:

$$\left[\frac{1}{v_g(\boldsymbol{r})}\frac{\partial}{\partial t}+\boldsymbol{\Omega}\cdot\nabla+\Sigma_{t,g}(\boldsymbol{r},t)\right]\psi_g(\boldsymbol{r},\boldsymbol{\Omega},t)=\int_{4\pi}\sum_{g'}\Sigma_{s,g'\to g}(\boldsymbol{r},\boldsymbol{\Omega}'\to\boldsymbol{\Omega},t)\psi_{g'}(\boldsymbol{r},\boldsymbol{\Omega}',t)\,d\boldsymbol{\Omega}'$$
$$+\frac{1}{k_{eff}}\left[\chi_{p,g}(\mathbf{r})\left(1-\sum_q\beta_q(\mathbf{r})\right)\sum_{g'}\nu\Sigma_{f,g'}(\mathbf{r},t)\phi_{g'}(\mathbf{r},t)+\sum_q\chi_{d,q,g}(\mathbf{r})\lambda_q C_q(\mathbf{r},t)\right] \quad (1)$$

$$\frac{\partial C_q(\boldsymbol{r},t)}{\partial t} = \beta_q(\boldsymbol{r}) \sum_{g'} \nu\Sigma_{f,g'}(\mathbf{r},t)\phi_{g'}(\boldsymbol{r},t) - \lambda_q C_q(\boldsymbol{r},t) \tag{2}$$

where ψ is the angular neutron flux, ϕ is the scalar neutron flux and C is the concentration of delayed-neutron precursors. The subscripts g and $g' = 1,\dots,G$ identify the energy groups and $q = 1,\dots,Q$ the families of precursors of delayed neutrons.

For steady-state conditions, the time derivatives in Eqs. (1) and (2) are zero and the static neutron flux $\psi_{g,0}(\boldsymbol{r},\boldsymbol{\Omega})$ satisfies the equation:

$$\left[\boldsymbol{\Omega}\cdot\nabla + \Sigma_{t,g,0}(\boldsymbol{r})\right]\psi_{g,0}(\boldsymbol{r},\boldsymbol{\Omega}) = \int_{4\pi}\sum_{g'}\Sigma_{s,g'\to g,0}(\boldsymbol{r},\boldsymbol{\Omega}'\to\boldsymbol{\Omega})\,\psi_{g',0}(\boldsymbol{r},\boldsymbol{\Omega}')d\boldsymbol{\Omega}'$$
$$+\frac{1}{\mathrm{k_{eff}}}\left[\chi_{\mathrm{p,g}}(\boldsymbol{r})\sum_{\mathrm{q}}\left(1-\beta_{\mathrm{q}}(\boldsymbol{r})\right)+\sum_{\mathrm{q}}\beta_{\mathrm{q}}(\boldsymbol{r})\right]\sum_{\mathrm{g'}}\nu\Sigma_{\mathrm{f,g',0}}(\boldsymbol{r},\mathrm{t})\phi_{\mathrm{g',0}}(\boldsymbol{r},\mathrm{t}) \tag{3}$$

The neutron noise equation in the frequency domain used for NOISE-SN is derived in the case that linear theory is valid. Small, stationary perturbations of the macroscopic nuclear cross sections are assumed to be induced by a possible disturbance in the reactor. The other system parameters, including $\mathrm{k_{eff}}$, are considered constant with respect to time. In the time-dependent equations, the neutron flux, the concentration of precursors and the nuclear cross sections are modelled as the sum of a static mean value and a fluctuating part. The static Eq. (3) is subtracted from Eqs. (1)-(2), the second-order perturbation terms are neglected, and a temporal Fourier transform is performed. Then, the neutron noise equation in the frequency domain reads as:

$$\left[\boldsymbol{\Omega}\cdot\nabla + \Sigma_{t,g,0}(\boldsymbol{r}) + \frac{i\omega}{v_g(\boldsymbol{r})}\right]\delta\psi_g(\boldsymbol{r},\boldsymbol{\Omega},\omega) = \int_{4\pi}\sum_{g'}\Sigma_{s,g'\to g,0}(\boldsymbol{r},\boldsymbol{\Omega}'\to\boldsymbol{\Omega})\,\delta\psi_{g'}(\boldsymbol{r},\boldsymbol{\Omega}',\omega)d\boldsymbol{\Omega}'$$
$$+\frac{1}{\mathrm{k_{eff}}}\left[\chi_{\mathrm{p,g}}(\boldsymbol{r})\sum_{\mathrm{q}}\left(1-\beta_{\mathrm{q}}(\boldsymbol{r})\right)+\sum_{\mathrm{q}}\chi_{\mathrm{d,q,g}}(\boldsymbol{r})\frac{\lambda_{\mathrm{q}}\beta_{\mathrm{q}}(\boldsymbol{r})}{i\omega+\lambda_{\mathrm{q}}}\right]\sum_{\mathrm{g'}}\nu\Sigma_{\mathrm{f,g',0}}(\boldsymbol{r})\delta\phi_{\mathrm{g'}}(\boldsymbol{r},\omega)+\mathrm{S_g}(\boldsymbol{r},\boldsymbol{\Omega},\omega) \tag{4}$$

The quantities $\delta\psi_g$ and $\delta\phi_{\mathrm{g}}$ are the induced angular and scalar neutron noise, respectively, and take complex values. The variable $\omega = 2\pi\mathrm{f}$ is the angular frequency of the driving perturbation. The imaginary unit is denoted as i. The term $\mathrm{S_g}(\boldsymbol{r},\boldsymbol{\Omega},\omega)$ in Eq. (4) is the neutron noise source, i.e.:

$$\mathrm{S_g}(\boldsymbol{r},\boldsymbol{\Omega},\omega) = -\delta\Sigma_{t,g}(\boldsymbol{r},\omega)\psi_{g,0}(\boldsymbol{r},\boldsymbol{\Omega}) + \int_{4\pi}\sum_{g'}\delta\Sigma_{s,g'\to g}(\boldsymbol{r},\boldsymbol{\Omega}'\to\boldsymbol{\Omega},\omega)\,\psi_{g',0}(\boldsymbol{r},\boldsymbol{\Omega}')d\boldsymbol{\Omega}'$$
$$+\frac{1}{\mathrm{k_{eff}}}\left[\chi_{\mathrm{p,g}}(\boldsymbol{r})\sum_{\mathrm{q}}\left(1-\beta_{\mathrm{q}}(\boldsymbol{r})\right)+\sum_{\mathrm{q}}\chi_{\mathrm{d,q,g}}(\boldsymbol{r})\frac{\lambda_{\mathrm{q}}\beta_{\mathrm{q}}(\boldsymbol{r})}{i\omega+\lambda_{\mathrm{q}}}\right]\sum_{\mathrm{g'}}\nu\delta\Sigma_{\mathrm{f,g'}}(\boldsymbol{r},\omega)\phi_{\mathrm{g',0}}(\boldsymbol{r}) \tag{5}$$

The quantity $\delta\Sigma$ is the perturbation associated with the generic nuclear cross section Σ.

Equations (4)-(5) correspond to a fixed source problem whose solution requires the effective multiplication factor $\mathrm{k_{eff}}$ and the neutron fluxes calculated under static conditions. Therefore, NOISE-SN consists of a static module and a module for the neutron noise simulations in the frequency domain.

2.2 Discretization of the equations

The static module in NOISE-SN solves the criticality problem given by Eq. (3). The discretization of the equation is based on a standard discrete ordinates method [11]. The angular flux is evaluated along discrete directions, and the scalar flux is constructed from the angular flux via the Legendre-Chebyshev quadrature set [12]. The spatial differencing relies on the diamond finite difference

method. Possible negative values of the neutron flux are corrected using the set-to-zero fixup. The neutron scattering term is approximated by an L-order real spherical harmonics expansion [13].

The frequency-domain neutron noise module calculates the complex-valued neutron noise induced by a neutron noise source prescribed in terms of nuclear cross-section fluctuations. The discretization of Eqs. (4)-(5) is similar to the static case. A set of discrete directions is selected, where the n-th discrete direction $\boldsymbol{\Omega_n}$ is defined by the direction cosines μ_n, η_n *and* ξ_n with respect to the orthogonal spatial coordinates (x, y, z). The equation is spatially discretized using the diamond finite difference method over a grid of rectangular cuboids. The centers of the grid cells are identified by triples of integer mesh indices (I, J, K) associated with the coordinates (x, y, z). The faces of the cells are given by triples where one half is added to or subtracted from the integer mesh index related to the direction perpendicular to the cell face. The volumes of the cells are $V_{I,J,K} = \Delta x_I \times \Delta y_J \times \Delta z_K$. Then, the discretized forms of Eqs. (4)-(5) read as:

$$\frac{\mu_n}{\Delta x_I}\left[\delta\psi_{g,n,I+1/2,J,K}(\omega) - \delta\psi_{g,n,I-1/2,J,K}(\omega)\right] + \frac{\eta_n}{\Delta y_J}\left[\delta\psi_{g,n,I,J+1/2,K}(\omega) - \delta\psi_{g,n,I,J-1/2,K}(\omega)\right]$$
$$+ \frac{\xi_n}{\Delta z_K}\left[\delta\psi_{g,n,I,J,K+1/2}(\omega) - \delta\psi_{g,n,I,J,K-1/2}(\omega)\right] + \left[\Sigma_{t,g,0,I,J,K} + \frac{i\omega}{v_{g,I,J,K}}\right]\delta\psi_{g,n,I,J,K}(\omega)$$
$$= \sum_{g'}\sum_{l=0}^{L}(2l+1)\Sigma_{sl,g'\to g,0,I,J,K}\sum_{m=-l}^{l} R_l^m(\boldsymbol{\Omega_n})\delta\phi^m_{l,g',I,J,K}(\omega)$$
$$+ \frac{1}{k_{eff}}\chi^{dyn}_{g,I,J,K}\sum_{g'}\nu\Sigma_{f,g',0,I,J,K}\delta\phi_{g',I,J,K}(\omega) + S_{g,n,I,J,K}(\omega) \tag{6}$$

and

$$S_{g,n,I,J,K}(\omega) = -\delta\Sigma_{t,g,I,J,K}(\omega)\psi_{g,n,I,J,K,0} + \sum_{g'}\sum_{l=0}^{L}(2l+1)\delta\Sigma_{sl,g'\to g,I,J,K}(\omega)\sum_{m=-l}^{l} R_l^m(\boldsymbol{\Omega_n})\phi^m_{l,g',I,J,K,0}$$
$$+ \frac{1}{k_{eff}}\chi^{dyn}_{g,I,J,K}\sum_{g'}\nu\delta\Sigma_{f,g',I,J,K}(\omega)\phi^{m=0}_{l=0,g',I,J,K,0} \tag{7}$$

In Eq. (6), the unknown is the angular neutron noise $\delta\psi_n$. For the closure of Eqs. (6)-(7), the diamond finite-difference relationships between the values at the centers and at the faces of a cell are used. In addition, the moments of the neutron noise $\delta\phi^m_{l,g,I,J,K}$ are obtained from the angular neutron noise with a quadrature formula. The expression of the noise source in Eq. (7) needs the static angular flux $\psi_{g,n,I,J,K,0}$, the flux moments $\phi^m_{l,g,I,J,K,0}$ and the effective multiplication k_{eff}, which are provided via the static module.

2.3 CMFD acceleration

A typical inner-outer iterative procedure is used for NOISE-SN to solve the static multi-energy-group neutron transport equations and the neutron noise equations. In an inner iteration, a transport sweep with respect to the discrete angular directions is performed to estimate the neutron fluxes for one energy group and construct the with-in group self-scattering term. After the inner iterations are completed from the highest to the lowest energy group, the neutron fluxes are used to evaluate the down-scattering term. Then, the fission source is updated in the outer iteration and a new set of inner iterations starts. The procedure is repeated until a convergence criterion is met.

When solving the neutron transport equation with an inner-outer iteration scheme, acceleration techniques are needed to improve the slow numerical convergence. The criticality calculations in the static module of NOISE-SN rely on a standard adCMFD acceleration method [14]. A similar algorithm is followed for the CMFD acceleration of the neutron noise calculations in the frequency domain. Details are discussed in [10].

2.4 Fictitious source method

In NOISE-SN, a fictitious source method can be used for the mitigation of the ray effects in 2-dimensional simulations. Accordingly, an additional, fictitious source term $\gamma S^{Fict}_{g,n,I,J}(\omega)$, which preserves the rotational invariance characteristic of the transport equation and converts the discrete ordinates equation to a spherical-harmonics-like equation [9], is added to the right-hand side of the 2-dimensional version of Eq. (6). The model of the fictitious source developed by Lathrop [15] is chosen and is coded following the algorithmic procedure described by Miller and Reed [16]. The factor γ can take values between 0 and 1 and allows to tune the strength of the fictitious source. If $\gamma = 0$, the original discrete ordinate equation is solved. If $\gamma = 1$, the mitigation of ray effects is expected to be maximum, but the convergence rate may worsen significantly. Details are reported in [10].

3 APOLLO3® neutron noise solver in the frequency domain

A neutron noise solver was developed in the IDT (Integral-Differential Transport) module of APOLLO3® deterministic code, developed at CEA, during the PhD thesis of A. Rouchon, before the beginning of the CORTEX project [17]. IDT is a lattice solver based on the Sn discrete ordinates method and on the method of short characteristics (MOSC). Since this solver has been often used in the project for verification and code-to-code comparison purposes (as detailed in Section 8), its main features are recalled in the following. A thorough description of the noise solver in IDT is provided in [17-18]. This solution scheme has also been implemented in a 2-D nodal diffusion solver of APOLLO3® based on the classical Nodal Expansion Method [18], but this implementation is not discussed here.

3.1 The noise equation

The equations solved by IDT are the linearized noise equations for the complex noise field $\delta\psi$ in the frequency domain, namely

$$\begin{aligned}\left(\boldsymbol{\Omega}\cdot\nabla+\Sigma_0(\mathbf{r},E)+i\frac{\omega}{\upsilon}\right)\delta\Psi(\mathbf{r},\boldsymbol{\Omega},E,\omega)&=\iint\Sigma_{0,s}(\mathbf{r},\boldsymbol{\Omega}'\cdot\boldsymbol{\Omega},E'\to E)\delta\Psi(\mathbf{r},\boldsymbol{\Omega}',E',\omega)dE'd\boldsymbol{\Omega}'\\&+\frac{1}{k}\frac{\chi_p(E)}{4\pi}\iint\nu_p(E')\Sigma_{0,f}(\mathbf{r},E')\delta\Psi(\mathbf{r},\boldsymbol{\Omega}',E',\omega)dE'd\boldsymbol{\Omega}'\\&+\frac{1}{k}\sum_j\frac{\chi_d^j(E)}{4\pi}\iint\nu_{d,\omega}^j(E')\Sigma_{0,f}(\mathbf{r},E')\delta\Psi(\mathbf{r},\boldsymbol{\Omega}',E',\omega)dE'd\boldsymbol{\Omega}'+S(\mathbf{r},\boldsymbol{\Omega},E,\omega),\end{aligned} \tag{8}$$

starting from a given noise source S. The discussion concerning the origin of this equation and the different operators appearing thereby is deferred to Section 6, in the context of the TRIPOLI-4® noise solver. The quantity ω represents the angular frequency. Notation is standard, and

$$\nu_{d,\omega}^j(E)=\left(\frac{\lambda_j^2-i\lambda_j\omega}{\lambda_j^2+\omega^2}\right)\nu_d^j(E), \tag{9}$$

is a shorthand for a frequency-dependent modified delayed neutron multiplicity. In IDT, the noise equation is split into a system of two equations for the real and imaginary part of the noise field $\delta\psi$. The two equations are formally coupled by two terms: the imaginary $1/v$ absorption cross section appearing at the left-hand side, and the modified delayed production operator including the complex multiplicity.

The noise source S is defined by:

$$S(\mathbf{r},\mathbf{\Omega},E,\omega) = -\delta\Sigma(\mathbf{r},E,\omega)\Psi_0(\mathbf{r},\mathbf{\Omega},E) + \iint \delta\Sigma_s(\mathbf{r},\mathbf{\Omega}'\cdot\mathbf{\Omega},E'\to E,\omega)\Psi_0(\mathbf{r},\mathbf{\Omega}',E')dE'd\mathbf{\Omega}'$$
$$+ \frac{1}{k}\frac{\chi_p(E)}{4\pi}\iint \nu_p(E')\delta\Sigma_f(\mathbf{r},E',\omega)\Psi_0(\mathbf{r},\mathbf{\Omega}',E')dE'd\mathbf{\Omega}'$$
$$+ \frac{1}{k}\sum_j \frac{\chi_d^j(E)}{4\pi}\iint \nu_{d,\omega}^j(E')\delta\Sigma_f(\mathbf{r},E',\omega)\Psi_0(\mathbf{r},\mathbf{\Omega}',E')dE'd\mathbf{\Omega}', \quad (10)$$

which depends on the model-specific functional forms of the Fourier-transformed perturbed cross sections $\delta\Sigma$ and on the stationary critical flux ψ_0. The noise equation and the source are dealt with in the framework of a multi-group transport description.

3.2 Basic features of the noise solver in IDT

In order to solve the frequency domain linearized noise equation with the deterministic code APOLLO3®, we apply the same iteration loops to the fission source (but the production operator is now complex) and to the scattering source as customary, and we add an iteration loop between the real and imaginary parts of the neutron noise equation to the solution of the one-group problem: details can be found in [17-18]. Thus, we can use the standard one-group diffusion or transport solver and consequently benefit from all numerical techniques that are already implemented in these one-group solvers. If needed, the noise source is computed by running a power iteration, in order to obtain the stationary critical flux ψ_0 and the associated fundamental eigenvalue k.

This solution scheme has been implemented in the IDT solver of APOLLO3®. The IDT solver is a lattice solver based on the Sn discrete ordinates method and on the method of short characteristics (MOSC). At the moment of writing this report, the 2-D neutron noise solver developed in APOLLO3® can be applied to homogeneous Cartesian geometries. Future work will concern the extension to heterogeneous Cartesian geometries.

4 APOLLO3®-IPK neutron noise solver in the time domain

The APOLLO3®-IPK neutron noise solver has been developed at CEA and used to simulate COLIBRI neutron noise experiments carried out at the CROCUS reactor [19].

4.1 Static simulations

Considering a heterogeneous reactor model with different pin displacements such as the CROCUS reactor in the COLIBRI experiments [20], see Figure 1, the TDT solver is used to compute the angular flux distributions solving the critical problem defined as:

$$\tilde{\Sigma}_t\psi(\vec{r},E,\Omega) = H\psi(\vec{r},E,\Omega) + \frac{1}{k}F_{tot}\phi(\vec{r},E), \quad (11)$$

where $\vec{r}$ is the spatial coordinate, E is the energy group, Ω is the direction angle, $\psi(\vec{r},E,\Omega)$ is the angular flux, $\phi(\vec{r},E)$ is the scalar flux, H is the scattering operator, F_{tot} is the total fission operator, k is the multiplication eigenvalue and $\tilde{\Sigma}_t$ is the equivalent total cross section of the problem. The value of the equivalent total cross section is defined as: $\tilde{\Sigma}_t(\vec{r},E) = \Sigma_t(\vec{r},E) + D(E)B^2$, where $\Sigma_t(\vec{r},E)$ is the total cross section from nuclear data and the $D(E)B^2$ is the leakage coefficient times the buckling value. The DB^2 term accounts for radial and axial leakage [21].

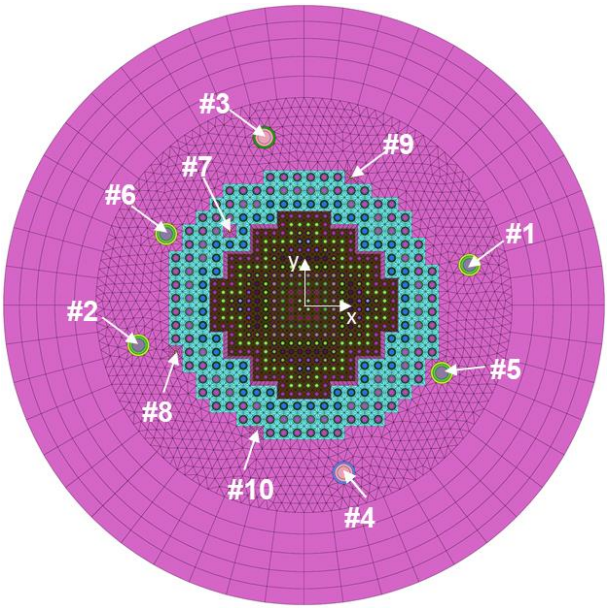

Figure 1: Computational mesh of the unperturbed CROCUS reactor and its detectors. The center XY of the coordinate reference system is also indicated.

4.2 The Improved Point-Kinetics – IPK noise model

Advancing from a previous work [22], the presented model aims at giving a more detailed representation of neutron noise in the CROCUS reactor during COLIBRI tests. The newly developed Improved Point-Kinetics (IPK) model solves the reactor kinetics problem using a multi-group energy discretization starting from the flux and precursors concentration equations:

$$\left(\frac{1}{v}\partial_t + \Omega\cdot\nabla + \tilde{\Sigma}_t(\vec{r},E,t)\right)\psi = H\psi + \frac{F_p}{k_{dyn}}\phi + \frac{F_d\vec{C}}{k_{dyn}} \tag{12}$$

$$\partial_t C_i(\vec{r},t) = -\bar{\lambda}_i C_i(\vec{r},t) + \beta_i \int_E dE'\,\nu\Sigma_f(\vec{r},E',t)\phi(\vec{r},E',t), \tag{13}$$

where $\tilde{\Sigma}_t(\vec{r},E,t)$ is the total cross section modified accounting for the DB^2 coefficient as determined in the static calculations, $\psi = \psi(\vec{r},E,\Omega,t)$ is the angular flux, $\phi = \phi(\vec{r},E,t)$ is the scalar flux, k_{dyn} is the dynamic eigenvalue [23] representative of the stationary oscillating regime calculated over the whole period of oscillation (T), Σ_f is the macroscopic fission cross section, ν is the average number of neutrons produced by fission, β_i is the fraction of delayed neutron for family i. The term F_p refers to the prompt fission operator and $F_d\vec{C} = \sum_{i=1}^{N_d}\chi_{d,i}\lambda_i C_i$ is the contribution from the neutron precursor concentration, with C_i containing the convolution integral for the *i*-th precursor family with decay constant λ_i. The delayed neutron source is integrated in time using a suitable quadrature formula to account for delayed-neutron contributions, as previously discussed in [23].

In the present model, differently from [24] and from the traditional quasi-static approach (e.g. [25]), in the angular flux factorization, the shape S and power P functions preserve their energy dependence and are defined according to:

$$\psi(\vec{r},E,\Omega,t) = S(\vec{r},E,\Omega,t)\cdot P(E,t). \tag{14}$$

The normalization condition adopted for all the energy groups N_G of the IPK model is defined as:

$$\frac{1}{v_g}\langle\psi^\dagger(\vec{r},E_g,\Omega',t), S(\vec{r},E_g,\Omega',t)\rangle = 1 \quad , \quad \forall t \wedge \forall g \in [1,N_G]. \tag{15}$$

where v_g is the neutron speed in group g.

To obtain the point-kinetics equations, Eq. (14) is multiplied by a weighting function $\psi^\dagger$ and integrated over space and angle (integration is denoted by $\langle \dots \rangle$) obtaining the general formulation of the problem:

$$\langle \psi^\dagger, \frac{1}{v}\partial_t \psi \rangle + \langle \psi^\dagger, \Omega \cdot \nabla \psi \rangle + \langle \psi^\dagger, \tilde{\Sigma}_t(\vec{r}, E, t)\psi \rangle = \langle \psi^\dagger, H\psi \rangle + \frac{1}{k_{dyn}} \langle \psi^\dagger, F_p \phi \rangle + \frac{1}{k_{dyn}} \langle \psi^\dagger, F_d \vec{C} \rangle. \quad (16)$$

In the present work, the weighting function is conveniently chosen as $\psi^\dagger = 1, \forall t \wedge \forall g \in [1, N_G]$ and, using the divergence theorem, the streaming term in Eq. (15) can be written for each energy group as:

$$\langle \psi^\dagger, \Omega \cdot \nabla \psi \rangle = \frac{J^+ - J^-}{\langle S/v \rangle} P. \quad (17)$$

With some manipulations, accounting for Eqs. (16) and (17), it is finally possible to obtain the balance point-kinetics equation for each energy group g:

$$\partial_t P + \frac{1}{v}\langle \partial_t S \rangle P + \frac{J^+ - J^-}{\langle S/v \rangle} P + \langle \tilde{\Sigma}_t S \rangle P - \langle HS \rangle P = \frac{1}{k_{dyn}} \langle F_p S \rangle P + \frac{1}{k_{dyn}} \langle F_d \vec{C} \rangle. \quad (18)$$

For the N initial computed static distributions, normalized according to Eq. (17), all flux points in the phase space $(\vec{x}, t)$, where $\vec{x} = (\vec{r}, E, \Omega)$, are interpolated in time over $M = L \times N$, with $L \in \mathbb{N}^+$, equally spaced points along the period, using a Fourier interpolation [26] of the kind:

$$S(\vec{x}, t) \cong c_0(\vec{x}) + \sum_{i=1}^{N/2} a_i(\vec{x}) \cos\left(\frac{2\pi}{T} t\right) + b_i(\vec{x}) \sin\left(\frac{2\pi}{T} t\right), \quad (19)$$

where the coefficients of the series (c_0, a_i and b_i) are obtained as:

$$c_0(\vec{x}) = \frac{1}{N} \sum_{j=1}^{N} S(\vec{x}, t_j), \quad (20)$$

$$a_i(\vec{x}) = \frac{2}{N} \sum_{j=1}^{N} S(\vec{x}, t_j) \cos\left(\frac{2\pi}{T} j \cdot t_j\right), \qquad j \neq N \quad (21)$$

$$a_N(\vec{x}) = \frac{1}{N} \sum_{j=1}^{N} S(\vec{x}, t_j) \cos\left(\frac{2\pi}{T} N \cdot t_j\right), \qquad j = N \quad (22)$$

$$b_i(\vec{x}) = \frac{2}{N} \sum_{j=1}^{N} S(\vec{x}, t_j) \sin\left(\frac{2\pi}{T} j \cdot t_j\right). \quad (23)$$

Concerning the temporal treatment, while the classical quasi-static method would imply the use of two different time scales for the solution of the equations for shape (coarse) and power (refined) [25], a single time scale is used to solve the transient. The final problem is a system of $M \times N_g$ equations to be solved iteratively using the power iteration method. With the converged $P(E, t)$, the angular flux is reconstructed and followed by the calculation and treatment of the detector responses.

The APOLLO3®-IPK neutron noise solver has been used to simulate COLIBRI experiments carried out at CROCUS and the results are presented in the CORTEX deliverable D2.5 [27].

5 A procedure for neutron noise calculations using a stochastic code

A Monte Carlo-based method, that allows estimating the neutron noise induced by stationary perturbations of macroscopic cross-sections in the frequency domain, has been developed at Chalmers. This method relies on the prior Monte Carlo computation of modified Green's functions associated to the real part of the dynamic macroscopic cross-sections, mimicking equivalent

subcritical problems driven by external neutron sources. Once such modified Green's functions are estimated, the neutron noise induced by any type of perturbations can be recovered, by solving a linear algebra problem accounting for the interdependence between the real and imaginary parts of the governing balance equations. A detailed description of the method can be found in [28].

5.1 Governing equations

For the sake of simplicity and illustration, the framework of diffusion theory with two energy groups is used. The balance equations in the frequency domain are obtained from the same procedure described in subsection 2.1 and read as:

$$\nabla\cdot\left[D_{1,0}\left(\mathbf{r}\right)\nabla\delta\phi_{1}\left(\mathbf{r},\omega\right)\right]+\left[\frac{\upsilon\Sigma_{f,1}\left(\mathbf{r},\omega\right)}{k_{eff}}-\Sigma_{1}\left(\mathbf{r},\omega\right)\right]\delta\phi_{1}\left(\mathbf{r},\omega\right)+\frac{\upsilon\Sigma_{f,2}\left(\mathbf{r},\omega\right)}{k_{eff}}\delta\phi_{2}\left(\mathbf{r},\omega\right)$$
$$=-\delta S_{1}\left(\mathbf{r},\omega\right) \tag{24}$$

$$\nabla\cdot\left[D_{2,0}\left(\mathbf{r}\right)\nabla\delta\phi_{2}\left(\mathbf{r},\omega\right)\right]+\Sigma_{r,0}\left(\mathbf{r}\right)\delta\phi_{1}\left(\mathbf{r},\omega\right)-\Sigma_{2}\left(\mathbf{r},\omega\right)\delta\phi_{2}\left(\mathbf{r},\omega\right)$$
$$=-\delta S_{2}\left(\mathbf{r},\omega\right) \tag{25}$$

with

$$\upsilon\Sigma_{f,1}\left(\mathbf{r},\omega\right)=\upsilon\Sigma_{f,1,0}\left(\mathbf{r}\right)\times\left(1-\frac{i\omega\beta}{i\omega+\lambda}\right) \tag{26}$$

$$\upsilon\Sigma_{f,2}\left(\mathbf{r},\omega\right)=\upsilon\Sigma_{f,2,0}\left(\mathbf{r}\right)\times\left(1-\frac{i\omega\beta}{i\omega+\lambda}\right) \tag{27}$$

$$\Sigma_{1}\left(\mathbf{r},\omega\right)=\Sigma_{a,1,0}\left(\mathbf{r}\right)+\frac{i\omega}{v_{1}}+\Sigma_{r,0}\left(\mathbf{r}\right) \tag{28}$$

$$\Sigma_{2}\left(\mathbf{r},\omega\right)=\Sigma_{a,2,0}\left(\mathbf{r}\right)+\frac{i\omega}{v_{2}} \tag{29}$$

$$\delta S_{1}\left(\mathbf{r},\omega\right)=\left[\frac{\delta\upsilon\Sigma_{f,1}\left(\mathbf{r},\omega\right)}{k_{eff}}\left(1-\frac{i\omega\beta}{i\omega+\lambda}\right)-\delta\Sigma_{a,1}\left(\mathbf{r},\omega\right)-\delta\Sigma_{r}\left(\mathbf{r},\omega\right)\right]\phi_{1,0}\left(\mathbf{r}\right)$$
$$+\frac{\delta\upsilon\Sigma_{f,2}\left(\mathbf{r},\omega\right)}{k_{eff}}\left(1-\frac{i\omega\beta}{i\omega+\lambda}\right)\phi_{2,0}\left(\mathbf{r}\right) \tag{30}$$

$$\delta S_2\left(\mathbf{r},\omega\right)=\delta\Sigma_r\left(\mathbf{r},\omega\right)\phi_{1,0}\left(\mathbf{r}\right)-\delta\Sigma_{a,2}\left(\mathbf{r},\omega\right)\phi_{2,0}\left(\mathbf{r}\right) \tag{31}$$

The Green's function technique can be used to solve the noise problem. The induced neutron noise is then given by integrals between the noise source $\delta S_{g'}(\boldsymbol{r}',\omega)$ and the Green's function $G_{g'\to g}(\boldsymbol{r},\boldsymbol{r}',\omega)$ with $g,g'=1,2$, i.e.:

$$\begin{bmatrix}\delta\phi_1\left(\mathbf{r},\omega\right)\\ \delta\phi_2\left(\mathbf{r},\omega\right)\end{bmatrix}=\begin{bmatrix}\int\left[G_{1\to1}\left(\mathbf{r},\mathbf{r}',\omega\right)\delta S_1\left(\mathbf{r}',\omega\right)+G_{2\to1}\left(\mathbf{r},\mathbf{r}',\omega\right)\delta S_2\left(\mathbf{r}',\omega\right)\right]d^3\mathbf{r}'\\ \int\left[G_{1\to2}\left(\mathbf{r},\mathbf{r}',\omega\right)\delta S_1\left(\mathbf{r}',\omega\right)+G_{2\to2}\left(\mathbf{r},\mathbf{r}',\omega\right)\delta S_2\left(\mathbf{r}',\omega\right)\right]d^3\mathbf{r}'\end{bmatrix} \tag{32}$$

The Green's function is evaluated by replacing the right-hand side of Eqs. (24) or (25) with Dirac-like perturbations $\delta(\boldsymbol{r}-\boldsymbol{r}')$.

5.2 Monte Carlo-based method

The neutron noise calculated via Eqs. (24)-(25) is a complex quantity. Conventional Monte Carlo transport codes are not designed to solve these types of complex-valued problems; however, the proposed method allows to avoid the limitation. In the current case, all the complex quantities in Eqs. (24)-(25) are split into a real part (denoted with the superscript r) and an imaginary part (denoted with the superscript i) and, after rearranging, the following system of equations is derived:

$$\mathbf{A}\left(\mathbf{r},\omega\right)\times\begin{bmatrix}\delta\phi_1^{\ }\left(\mathbf{r},\omega\right)\\ \delta\phi_2^{\ }\left(\mathbf{r},\omega\right)\end{bmatrix}=-\begin{bmatrix}\delta S_1^{\ }\left(\mathbf{r},\omega\right)\\ \delta S_2^{\ }\left(\mathbf{r},\omega\right)\end{bmatrix}-i\mathbf{B}\left(\mathbf{r},\omega\right)\times\begin{bmatrix}\delta\phi_1^{\ }\left(\mathbf{r},\omega\right)\\ \delta\phi_2^{\ }\left(\mathbf{r},\omega\right)\end{bmatrix} \tag{33}$$

The matrix $\boldsymbol{A}(\boldsymbol{r},\omega)$ and $\boldsymbol{B}(\boldsymbol{r},\omega)$ are respectively equal to:

$$\mathbf{A}\left(\mathbf{r},\omega\right)=\begin{bmatrix}\nabla\cdot\left[D_{1,0}\left(\mathbf{r}\right)\nabla\right]+\dfrac{\upsilon\Sigma_{f,1}^{r}\left(\mathbf{r},\omega\right)}{k_{eff}}-\Sigma_1^r\left(\mathbf{r},\omega\right) & \dfrac{\upsilon\Sigma_{f,2}^{r}\left(\mathbf{r},\omega\right)}{k_{eff}}\\ \Sigma_{r,0}\left(\mathbf{r}\right) & \nabla\cdot\left[D_{2,0}\left(\mathbf{r}\right)\nabla\right]-\Sigma_2^r\left(\mathbf{r},\omega\right)\end{bmatrix} \tag{34}$$

$$\mathbf{B}\left(\mathbf{r},\omega\right)=\begin{bmatrix}\dfrac{\upsilon\Sigma_{f,1}^{i}\left(\mathbf{r},\omega\right)}{k_{eff}}-\Sigma_1^i\left(\mathbf{r},\omega\right) & \dfrac{\upsilon\Sigma_{f,2}^{i}\left(\mathbf{r},\omega\right)}{k_{eff}}\\ 0 & -\Sigma_2^i\left(\mathbf{r},\omega\right)\end{bmatrix} \tag{35}$$

Equation (33) can be solved using the Green's function technique. Accordingly, the right-hand side of Eq. (33) is replaced by a Dirac-like perturbation $\delta(\boldsymbol{r}-\boldsymbol{r}')$ in either the thermal or the fast energy group and the so-called modified Green's function $\tilde{G}_{g'\to g}(\boldsymbol{r},\boldsymbol{r}',\omega)$ is estimated. The solution to the original neutron noise problem described by Eq. (33) is then obtained from integrals including the actual right-hand side of Eq. (33), denoted as $\widetilde{\delta S}_{g'}(\boldsymbol{r}',\omega)$ with $g'=1,2$, and the modified Green's function $\tilde{G}_{g'\to g}(\boldsymbol{r},\boldsymbol{r}',\omega)$, i.e.:

$$\begin{bmatrix}\delta\phi_1\left(\mathbf{r},\omega\right)\\ \delta\phi_2\left(\mathbf{r},\omega\right)\end{bmatrix}=\begin{bmatrix}\int\left[\widetilde{G}_{1\to1}\left(\mathbf{r},\mathbf{r}',\omega\right)\widetilde{\delta S}_1\left(\mathbf{r}',\omega\right)+\widetilde{G}_{2\to1}\left(\mathbf{r},\mathbf{r}',\omega\right)\widetilde{\delta S}_2\left(\mathbf{r}',\omega\right)\right]d^3\mathbf{r}'\\ \int\left[\widetilde{G}_{1\to2}\left(\mathbf{r},\mathbf{r}',\omega\right)\widetilde{\delta S}_1\left(\mathbf{r}',\omega\right)+\widetilde{G}_{2\to2}\left(\mathbf{r},\mathbf{r}',\omega\right)\widetilde{\delta S}_2\left(\mathbf{r}',\omega\right)\right]d^3\mathbf{r}'\end{bmatrix} \tag{36}$$

with

$$\begin{bmatrix}\widetilde{\delta S}_1\left(\mathbf{r}',\omega\right)\\ \widetilde{\delta S}_2\left(\mathbf{r}',\omega\right)\end{bmatrix}=-\begin{bmatrix}\delta S_1\left(\mathbf{r}',\omega\right)\\ \delta S_2\left(\mathbf{r}',\omega\right)\end{bmatrix}-i\mathbf{B}\left(\mathbf{r}',\omega\right)\times\begin{bmatrix}\delta\phi_1\left(\mathbf{r}',\omega\right)\\ \delta\phi_2\left(\mathbf{r}',\omega\right)\end{bmatrix} \tag{37}$$

The Green's function $\tilde{G}_{g'\to g}(\boldsymbol{r},\boldsymbol{r}',\omega)$ is different from the Green's function $G_{g'\to g}(\boldsymbol{r},\boldsymbol{r}',\omega)$ used in Eq. (32) to solve the original set of Eqs. (24)-(25). In particular, the modified Green's function $\tilde{G}_{g'\to g}(\boldsymbol{r},\boldsymbol{r}',\omega)$ is real, whereas the Green's function $G_{g'\to g}(\boldsymbol{r},\boldsymbol{r}',\omega)$ is complex. The main advantage of reformulating the solution from Eq. (32) to Eq. (36) lies with the fact that the reaction rates appearing in the matrix $\boldsymbol{A}(\boldsymbol{r},\omega)$ are all real and it could be demonstrated that those reaction rates have the same sign as when solving the problem of a subcritical system. The modified Green's function $\tilde{G}_{g'\to g}(\boldsymbol{r},\boldsymbol{r}',\omega)$ can thus be determined using Monte Carlo techniques, as long as the macroscopic cross-sections can be specified using cross-section files in a proper format [20].

Because of the spatial variables $\boldsymbol{r}$ and $\boldsymbol{r}'$ appearing in the modified Green's function $\tilde{G}_{g'\to g}(\boldsymbol{r},\boldsymbol{r}',\omega)$, a spatial discretization of the system being modelled is required prior to computing the modified Green's functions. Then the system has to be replaced by a set of homogenized regions using properly averaged macroscopic cross sections. The proposed method is similar to the fission matrix method used in Monte Carlo simulations, where the production of neutrons in a given homogenized region due to neutrons born in any homogenized region is determined. After the spatial discretization, Eqs. (36) and (37) can be recast into:

$$\boldsymbol{\delta\phi}\left(\omega\right)=-\widetilde{\mathbf{G}}\left(\omega\right)\times\boldsymbol{\delta\mathbf{S}}\left(\omega\right)-i\widetilde{\mathbf{G}}\left(\omega\right)\times\mathbf{B}\left(\omega\right)\times\boldsymbol{\delta\phi}\left(\omega\right) \tag{38}$$

All the quantities in the equation above are generically vectors and matrices taking both the spatial and energy discretization of all balance equations into account. In the end, Eq. (38) is rewritten as:

$$\left[\mathbf{I}+i\widetilde{\mathbf{G}}\left(\omega\right)\times\mathbf{B}\left(\omega\right)\right]\times\boldsymbol{\delta\phi}\left(\omega\right)=-\widetilde{\mathbf{G}}\left(\omega\right)\times\boldsymbol{\delta\mathbf{S}}\left(\omega\right) \tag{39}$$

Equation (39) is a linear system of equations that can be solved once the discretized modified Green's functions $\tilde{G}_{g'\to g}(\boldsymbol{r},\boldsymbol{r}',\omega)$ have been determined from a Monte Carlo code. Therefore, the coupling between the real and imaginary parts of the induced neutron noise is resolved externally to the Monte Carlo simulations.

6 TRIPOLI-4® neutron noise solver

TRIPOLI-4® is the reference Monte Carlo code developed at CEA [29]. A frequency-domain noise solver was implemented in TRIPOLI-4® for the purposes of the CORTEX project, based on previous work on a prototype Monte Carlo code [30]. The basic implementation details are sketched in [31] and the treatment of the "noise source" corresponding to mechanical vibrations is dealt with in [32]. The key ideas of the solver and the overall simulation strategy are largely inspired by the findings of Amélie Rouchon's PhD thesis [17], based on the pioneering contributions of [33]. In the following, we provide an overview of the noise solver and detail its main features.

6.1 Overall computational strategy

We briefly review the noise equations in the frequency domain, in order to provide a coherent framework, and then detail how TRIPOLI-4® solves these equations.

6.1.1 The noise equations in the frequency domain

The version of the noise equations that TRIPOLI-4® solves by the Monte Carlo method corresponds to the so-called orthodox linearization of the Fourier-transformed exact noise equations. The *exact* noise equations for the frequency-domain neutron noise $\delta\varphi(\omega) = \delta\varphi(\mathbf{r}, \mathbf{\Omega}, E, \omega)$ read

$$\mathcal{B}(\omega)\delta\varphi(\omega) + \frac{1}{2\pi}\int \delta\mathcal{B}(\omega-\omega')\delta\varphi(\omega')d\omega' = -\delta\mathcal{B}(\omega)\varphi_c \tag{40}$$

where

$$\begin{aligned}\mathcal{B}(\omega) = i\frac{\omega}{v} + \Sigma_t(\mathbf{r},E) + \mathbf{\Omega}\cdot\nabla - \int\int f_s(\mathbf{\Omega}'\cdot\mathbf{\Omega}, E'\to E)\Sigma_s(\mathbf{r},E')dE'd\mathbf{\Omega}' \\ - \frac{\chi_p(E)}{4\pi k_{\text{eff}}}\int\int \nu_p(E')\Sigma_f(\mathbf{r},E')dE'd\mathbf{\Omega}' \\ - \sum_j \frac{\lambda_j}{\lambda_j+i\omega}\frac{\chi_d^j(E)}{4\pi k_{\text{eff}}}\int\int \nu_d^j(E')\Sigma_f(\mathbf{r},E')dE'd\mathbf{\Omega}'\end{aligned} \tag{41}$$

is the Fourier-transformed Boltzmann operator (notation is as customary, and ω denotes the angular frequency), $\varphi_c(\mathbf{r}, \mathbf{\Omega}, E)$ is the critical flux satisfying the k-eigenvalue Boltzmann equation (having associated fundamental eigenvalue k_{eff}), and

$$\begin{aligned}\delta\mathcal{B}(\omega) = \delta\Sigma_t(\mathbf{r},E,\omega) - \int\int f_s(\mathbf{\Omega}'\cdot\mathbf{\Omega}, E'\to E)\delta\Sigma_s(\mathbf{r},E',\omega)dE'd\mathbf{\Omega}' \\ - \frac{\chi_p(E)}{4\pi k_{\text{eff}}}\int\int \nu_p(E')\delta\Sigma_f(\mathbf{r},E',\omega)dE'd\mathbf{\Omega}' \\ - \sum_j \frac{\lambda_j}{\lambda_j+i\omega}\times\frac{\chi_d^j(E)}{4\pi k_{\text{eff}}}\int\int \nu_d^j(E')\delta\Sigma_f(\mathbf{r},E',\omega)dE'd\mathbf{\Omega}'.\end{aligned} \tag{42}$$

is the perturbation operator. The terms $\delta\Sigma_\alpha(\boldsymbol{r}, E, \omega)$ appearing in the perturbation operator express the Fourier-transformed cross section perturbations for a given reaction α, and depend on the specific noise model (this point will be illustrated in the following). The *orthodox linearization* consists in neglecting the product of perturbed quantities, which yields the linearized noise equation in the frequency domain, namely,

$$\mathcal{B}(\omega)\delta\varphi(\omega) = -\delta\mathcal{B}(\omega)\varphi_c \tag{43}$$

Formally speaking, the linearized noise equation has the structure of a fixed-source transport equation for the unknown noise field $\delta\varphi(\omega) = \delta\varphi(\mathbf{r}, \mathbf{\Omega}, E, \omega)$, where - $\delta B(\omega)\ \varphi_c(\mathbf{r}, \mathbf{\Omega}, E)$ is the "noise source" and $B(\omega)$ is the transport operator. Observe that both $B(\omega)$ and $\delta\varphi(\omega)$ are complex quantities. The impact of considering the linearized noise equation instead of the exact noise equation in the frequency domain has been thoroughly discussed in [32]. From now on, we will focus exclusively on the linearized noise equation, which is precisely the equation that is solved by TRIPOLI-4®.

6.1.2 Computational strategy

In view of the structure of the linearized noise equation, the solution strategy by Monte Carlo method is the following:

1. First, determine the critical flux $\varphi_c(\mathbf{r}, \mathbf{\Omega}, E)$, which can be achieved by running a regular power iteration with a sufficient number of inactive cycles, starting from an arbitrary neutron distribution.
2. Once the neutron population is distributed according to $\varphi_c(\mathbf{r}, \mathbf{\Omega}, E)$, sample the noise source - $\delta B(\omega)\, \varphi_c(\mathbf{r}, \mathbf{\Omega}, E)$. The operator $\delta B(\omega)$ must be prepared before running the simulation and depends on the specific noise problem under consideration, since it contains the Fourier-transformed perturbed cross sections $\delta\Sigma_\alpha(\omega)$. Typical functional forms of the perturbed cross sections $\delta\Sigma_\alpha(\omega)$ will be discussed later on, for oscillations and mechanical vibrations.
3. Since $\delta B(\omega)$ is in general complex, the noise source stemming from - $\delta B(\omega)\, \varphi_c(\mathbf{r}, \mathbf{\Omega}, E)$ will be also complex: this means that the resulting particle population must carry two weights, one for the real part and one for the imaginary part, each having a sign.
4. The particle population must be transported by following the stochastic rules imposed by the operator $B(\omega)$, in order to determine the noise field $\delta\varphi(\omega)$. Since $B(\omega)$ closely resembles the regular Boltzmann operator, up to slight frequency-dependent modifications, we will show that it is possible to solve the transport problem associated to $B(\omega)$ by a set of stochastic rules that can be obtained by suitably modifying those associated to the regular Boltzmann operator.
5. Independent replicas over a collection of M batches will ensure that error bars on the noise field $\delta\varphi(\omega)$ can be correctly estimated.

The overall computational scheme, including the preparation of critical eigenstate, the sampling of the noise source and the propagation of the noise particles, is synthetized in Figure 2.

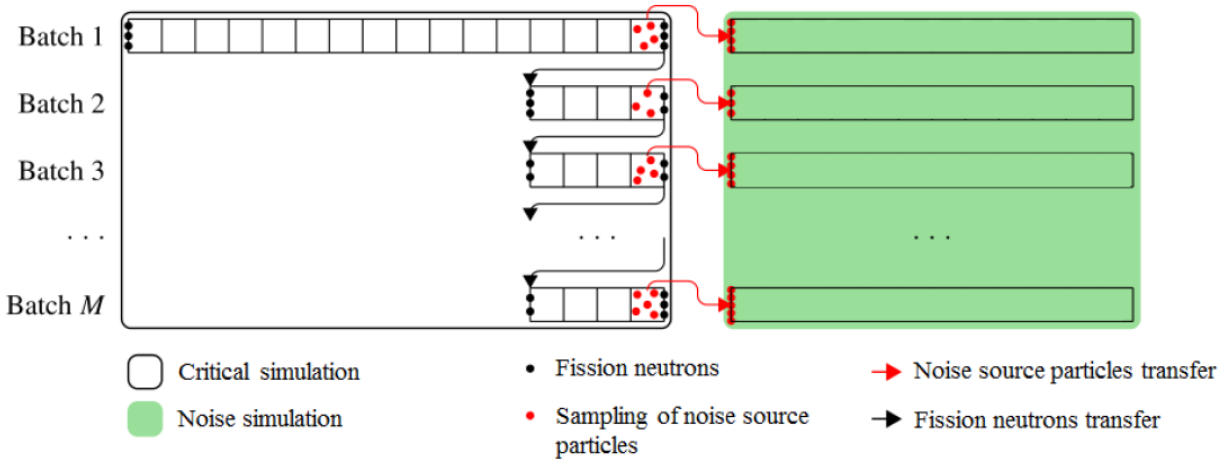

Figure 2: Overall computational scheme used in TRIPOLI-4®.

A complete power iteration is performed once in the first batch: during the final cycle noise source particles are sampled so that the noise simulation can begin, while the generated fission neutrons are transferred to the second batch. This latter runs a few additional inactive cycles in order to ensure reasonable decorrelation between cycles before sampling the noise source for the second replica. The third batch gets the fission neutrons generated by the second one, and so on. In a parallel run, each processor would apply this strategy.

6.2 Sampling the noise source

The noise source models currently available in TRIPOLI-4® cover oscillations and mechanical vibrations, whose assumptions and explicit expressions are recalled in the following.

6.2.1 Oscillations

For the case of oscillations, which would be an adequate model to represent, e.g., the effects of temperature-induced modifications of the cross sections (as in the case of absorbers of variable strength), without any spatial movement, the perturbed cross sections in the time domain are assumed to be of the form

$$\delta\Sigma_x(r,E,t) = \quad \varepsilon \quad \times \Sigma_{0,x}(r,E)\cos(\omega_0 t) \tag{44}$$

where Σ_0 is the non-perturbed cross section, ε is the amplitude of the perturbation and ω_0 is the frequency of the perturbation. Then, by using the Fourier transform

$$\mathcal{F}[\sin(\omega_0 t)] = -i\pi[\delta(\omega-\omega_0)-\delta(\omega+\omega_0)] \tag{45}$$

the expression for the perturbed cross section on the frequency domain is readily obtained. The resulting noise source is thus monochromatic, at frequency ω_0, and we thus expect the induced noise field $\delta\varphi(\omega)$ to be also monochromatic at frequency ω_0, i.e., $\delta\varphi(\omega) = \delta\varphi(\omega_0)$, due to the linearity of the noise equations that are solved by TRIPOLI-4®.

6.2.2 Mechanical vibrations

Let us now assume that the neutron noise is induced by one or several vibrating interfaces between homogeneous materials. We will focus on the case where the vibration acts along a single axis, say x, and let us denote by x_0 the unperturbed position of the interface. We define $\Sigma_\alpha^L(E)$ and $\Sigma_\alpha^R(E)$ the spatially homogeneous cross sections of the regions at the left ($x < x_0$) and the right ($x > x_0$), respectively, of the interface at x_0. We assume that the vibration is periodic, with frequency ω_0 and period $T_0 = 2\pi / \omega_0$, and with amplitude ε smaller than the linear size d of the region concerned by the interface perturbation. The position of the moving interface will be described by

$$x_i(t) = x_0 + \varepsilon\sin(\omega_0 t) \tag{46}$$

with

$$x_0 - \varepsilon < x_i(t) < x_0 + \varepsilon. \tag{47}$$

Under these assumptions, the general form of the interface perturbation in the time domain is

$$\delta\Sigma_\alpha(x,E,t) = \Delta\Sigma_\alpha(E)[H(x-x_0) - H(x-x_0-\varepsilon\sin(\omega_0 t))], \tag{48}$$

where

$$\Delta\Sigma_\alpha(E) = \Sigma_\alpha^L(E) - \Sigma_\alpha^R(E) \tag{49}$$

and $H(z)$ is the Heaviside function, with $H(z) = 1$ for $z \geq 0$, and $H(z) = 0$ otherwise. Observe that $\delta\Sigma_\alpha(x,E,t)$ is non-zero only in the region traversed by the vibrating interface, namely, $x_0 - \varepsilon \leq x \leq x_0 - \varepsilon$.

Let us first consider the region x > x0, where

$$\begin{aligned}\delta\Sigma_\alpha^R(x,E,t) &= \Delta\Sigma_\alpha(E)[1 - H(x-x_0-\varepsilon\sin(\omega_0 t))] \\ &= \Delta\Sigma_\alpha(E)H(\varepsilon\sin(\omega_0 t) - x + x_0).\end{aligned} \tag{50}$$

In this case, the Heaviside function is equal to unity when

$$\sin(\omega_0 t) \geqslant \frac{x-x_0}{\varepsilon}, \tag{51}$$

and zero otherwise, i.e., between time

$$\tau(x,x_0) = \frac{1}{\omega_0}\arcsin\left(\frac{x-x_0}{\varepsilon}\right) \tag{52}$$

and

$$T_0/2 - \tau(x, x_0) = \pi/\omega_0 - \tau(x, x_0). \tag{53}$$

This condition yields a rectangular wave

$$\delta\Sigma_\alpha^R(x, E, t) = \Delta\Sigma_\alpha(E)\left[\frac{1}{2} - \frac{\omega_0\tau(x, x_0)}{\pi} + 2\sum_{n=1}^{\infty}\frac{\sin\left(\frac{n\pi}{2} - n\omega_0\tau(x, x_0)\right)}{n\pi}\cos\left(\frac{n\pi}{2} - n\omega_0 t\right)\right], \tag{54}$$

whose Fourier transform yields

$$\delta\Sigma_\alpha^R(x, E, \omega) = \Delta\Sigma_\alpha(E)\left\{c_0^R(x, x_0)\delta(\omega) + \sum_{n=1}^{\infty}c_n^R(x, x_0)\left[\delta(\omega - n\omega_0) + \delta(\omega + n\omega_0)e^{in\pi}\right]\right\}. \tag{55}$$

This equation defines an infinite sum of contributions corresponding to discrete frequencies $\pm n\omega_0$ with $n = 0,1, \ldots$, multiple of the fundamental frequency ω_0. The space-dependent Fourier coefficients are given by

$$c_0^R(x, x_0) = \pi - 2\omega_0\tau(x, x_0) = \pi - 2\arcsin\left(\frac{x - x_0}{\varepsilon}\right) \tag{56}$$

and

$$c_n^R(x, x_0) = 2\frac{\sin\left(\frac{n\pi}{2} - n\omega_0\tau(x, x_0)\right)}{n}e^{-in\frac{\pi}{2}} = 2\frac{\sin\left(n\arccos\left(\frac{x - x_0}{\varepsilon}\right)\right)}{n}e^{-in\frac{\pi}{2}} \tag{57}$$

for $n \geq 1$, whose amplitude decreases with increasing n. In particular, the coefficient corresponding to the first harmonic at ω_0 is negative and imaginary:

$$c_1^R(x, x_0) = -2i\sqrt{1 - \left(\frac{x - x_0}{\varepsilon}\right)^2}; \tag{58}$$

for the second harmonic at $2\omega_0$ the coefficient is negative and real:

$$c_2^R(x, x_0) = -2\left(\frac{x - x_0}{\varepsilon}\right)\sqrt{1 - \left(\frac{x - x_0}{\varepsilon}\right)^2}. \tag{59}$$

More generally, all odd coefficients are imaginary, and all even coefficients are real.

For the region $x < x_0$, we have

$$\delta\Sigma_\alpha^L(x, E, t) = -\Delta\Sigma_\alpha(E)H(x - x_0 - \varepsilon\sin(\omega_0 t)). \tag{60}$$

In this case, the Heaviside function is equal to unity when

$$\sin(\omega_0 t) \leqslant \frac{x - x_0}{\varepsilon}, \tag{61}$$

and zero otherwise, i.e., between time $T_0/2 + \tau(x, x_0)$ and $T_0 - \tau(x, x_0)$. This condition defines a rectangular wave that is shifted by $T_0/2$ with respect to the one for the region $x > x_0$. By applying the Fourier transform, we have thus

$$\delta\Sigma_\alpha^L(x,E,\omega) = \Delta\Sigma_\alpha(E) \times\left\{c_0^L(x,x_0)\delta(\omega)+\sum_{n=1}^{\infty}c_n^L(x,x_0)\left[\delta(\omega-n\omega_0)+\delta(\omega+n\omega_0)e^{in\pi}\right]\right\}, \tag{62}$$

where

$$c_n^L(x,x_0) = c_n^R(x,x_0) \tag{63}$$

for $n \geq 1$, and

$$c_0^L(x,x_0) = c_0^R(x,x_0) - 2\pi. \tag{64}$$

The spatial behavior of the exact noise source is illustrated in Figure 3.

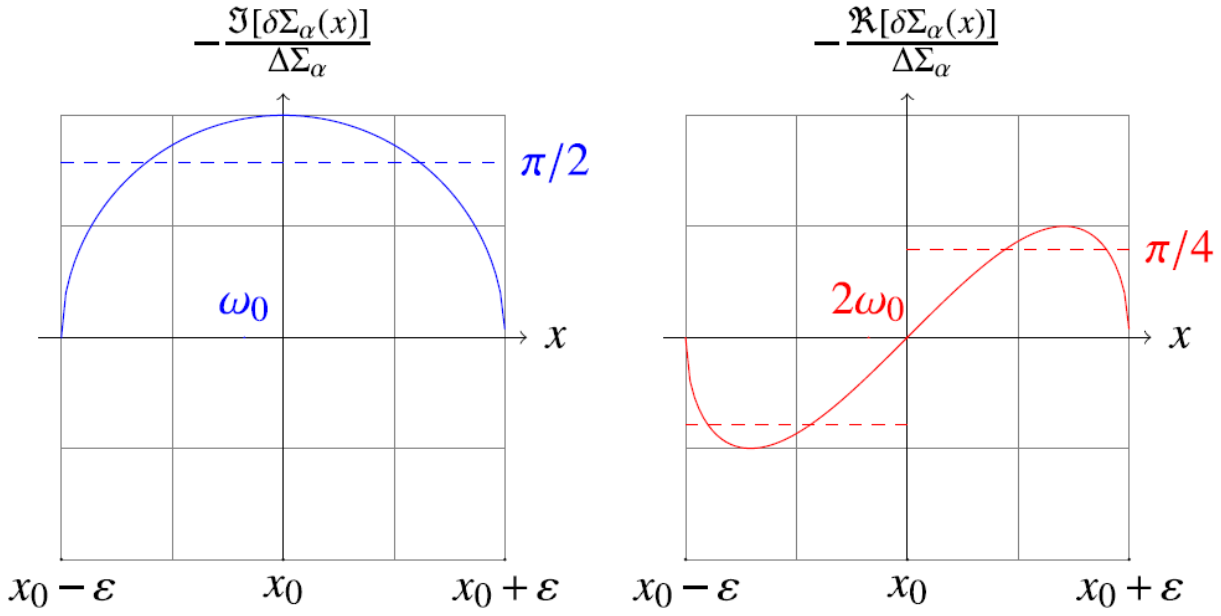

Figure 3: The spatial shape of the noise source. Comparison between the exact representation used in TRIPOLI-4® (plotted as solid line) and the ε/d approximation (plotted as a dashed line, using the nascent functions to represent the singular spatial behavior located at the interface), see details in [32]. Left: the imaginary part of the component at ω_0; right: the real part of the component at $2\omega_0$.

So far, we have examined a single vibrating interface. The case of a region of size d vibrating into a host material can be dealt with by considering the linear superposition of the effects of two vibrating interfaces, each located at the boundaries of the region. In this case, the terms corresponding to the respective boundaries will have opposite signs, so that one might possibly expect interference phenomena due to the simultaneous presence of two vibrating interfaces. The intensity of the interference of the interfaces will depend on the interplay between the vibration amplitude ε and the linear separation d between the boundaries: these effects are thoroughly discussed in [32].

The previous equations completely define the Fourier spectrum of the noise source corresponding to a vibrating boundary between two homogeneous regions, for a sinusoidal displacement at a single frequency ω_0. By virtue of the functional form of the noise source, the system will in principle respond to the vibration at several discrete frequencies $n\omega_0$, despite the impulsion being monochromatic at ω_0. The noise response $\delta\varphi(\omega)$ for a given discrete frequency $\omega_n = n\omega_0$ will depend on the source intensity, i.e., on the space-dependent Fourier coefficients and on the shape of the fundamental flux $\varphi_c(\mathbf{r}, \mathbf{\Omega}, E)$. The noise source term for mechanical vibrations can be generally written as

$$-\delta\mathcal{B}(\omega)\varphi_c = -\sum_n \delta\mathcal{B}_n\varphi_c\delta(\omega-n\omega_0), \tag{65}$$

with the appropriate noise source components δB_n associated to the cross-section perturbations, to be inferred by the previous definitions of the Fourier coefficients in the expressions of $\delta B(\omega)$. We thus expect the noise field $\delta\varphi(\omega)$ to be of the form

$$\delta\varphi(\mathbf{r},\mathbf{\Omega},E,\omega)=\sum_n \delta\varphi_n(\mathbf{r},\mathbf{\Omega},E)\delta(\omega-n\omega_0), \tag{66}$$

where $\delta\varphi_n$ solve

$$\mathcal{B}_n\delta\varphi_n=-\delta\mathcal{B}_n\varphi_c, \tag{67}$$

i.e., an infinite system of fully decoupled linearized noise equations. Here we have denoted the noise operator by $B_k = B(\omega=\omega_k)$ and the perturbation operator by $\delta B_k = \delta B(\omega=\omega_k)$, respectively, evaluated at the discrete frequencies $k\omega_0$ of the source. TRIPOLI-4® solves each contribution separately, for the chosen index n of the noise harmonic. In practice, only the first few components are computed (see the discussion in [32] concerning the relevance of the higher harmonics). The noise source contributions due to negative frequencies $n < 0$ can be dealt with by observing that

$$\delta\varphi_{-n}=\delta\varphi_n^{\dagger}, \tag{68}$$

where the dagger symbol denotes complex conjugation. Finally, the noise source contribution at $n = 0$, which corresponds to $\omega = 0$ (i.e., the time-average of the perturbation), physically represents the offset due to the fact that the perturbation will in general introduce a non-vanishing reactivity effect in the system. For the linearized noise equations all the components are decoupled from each other, so that the equation for $n = 0$ will not influence the others and can be disregarded when solving for $n \geq 1$.

6.2.3 Sampling methods

For both the oscillation and the vibration model, the resulting noise source $-\delta B(\omega)\,\varphi_c(\mathbf{r}, \mathbf{\Omega}, E)$ is a complex function depending on the stationary flux $\varphi_c(\mathbf{r}, \mathbf{\Omega}, E)$. As mentioned, a standard power iteration is first run in order for the neutron population to be distributed according to the critical flux $\varphi_c(\mathbf{r}, \mathbf{\Omega}, E)$. The fundamental k-eigenvalue is simultaneously determined. The noise source for a given frequency $k\omega_0$ is then sampled by weighting the 'noise particles' associated by each component of $\delta B(\omega)$ by the stationary collision density associated to $\varphi_c(\mathbf{r}, \mathbf{\Omega}, E)$. For instance, for the prompt fission term we would have

$$\frac{1}{k}\frac{\chi_p(E)}{4\pi}\iint \nu_p(E')\frac{\delta\Sigma_{0,f}(\boldsymbol{r},E',\omega)}{\Sigma_{0,f}(\boldsymbol{r},E')}\Sigma_{0,f}(\boldsymbol{r},E')\varphi_c(\boldsymbol{r},\mathbf{\Omega}',E')dE'd\mathbf{\Omega}' \tag{69}$$

which means that at fission events we would instantiate ν_p/k 'noise particles' with spectrum $\chi_p(E)$ and with a (generally complex) statistical weight multiplier $\delta\Sigma_f(\boldsymbol{r},E',\omega)/\Sigma_{0,f}(\boldsymbol{r},E')$ depending on the specific perturbation. Observe that the eigenvalue k must be also known, in addition to the fundamental mode φ_c. The delayed fission term contains an additional weight multiplier, depending on the frequency and on the decay constants of the precursors: this factor can be interpreted as an effective frequency-dependent delayed neutron yield

$$\nu_{d,\omega}^{j}(E)=\left(\frac{\lambda_j^2-i\lambda_j\omega}{\lambda_j^2+\omega^2}\right)\nu_d^j(E) \tag{70}$$

which can be readily transformed into a weight multiplier. More generally, all the terms of the noise source can be written as

$$f_r(\mathbf{\Omega},E\rightarrow\mathbf{\Omega}',E')\times\frac{\delta\Sigma_r(\mathbf{r},E,\omega)}{\Sigma_r(\mathbf{r},E)}\times\Sigma_r(\mathbf{r},E)\,\varphi_c(\mathbf{r},\mathbf{\Omega},E) \tag{71}$$

which have the form of a production rate (associated to the event "r") with a weight multiplier involving the Fourier-transformed cross section perturbations and possibly a frequency-dependent yield.

Consequently, the resulting noise source will be composed by a collection of particles being produced with rate $\Sigma_r \varphi_c$, having a spectrum f_r, and a complex weight

$$w(\omega) = \{w_{\Re}(\omega), w_{\Im}(\omega)\} \tag{72}$$

where the *signs* of the real and imaginary parts of particle weights can be *positive or negative*.

6.3 Solving the linearized noise equations

Suppose now that the noise source $-\delta B(\omega)\,\varphi_c(\mathbf{r}, \mathbf{\Omega}, E)$ has been sampled by the procedures described above. We want now to solve the linearized noise equation

$$\mathcal{B}_n \delta\varphi_n = -\delta\mathcal{B}_n \varphi_c, \tag{73}$$

for a collection of discrete frequencies $n\omega_0$ of the source. We recall that $B_n = B(\omega=\omega_n)$ and $\delta B_n = \delta B(\omega=\omega_n)$ denote respectively the noise operator and the perturbation operator, evaluated at the discrete frequencies. The operator $B(\omega=\omega_n)$ is basically a modified Boltzmann operator, containing additional complex terms. In [30] we have suggested a sampling scheme to estimate $\delta\varphi_n$ by Monte Carlo sampling, and this strategy has been later implemented in TRIPOLI-4® for the CORTEX project [31]. In the following, we will sketch the basic principles of the involved methods.

6.3.1 Sampling strategy

The operator $B(\omega=\omega_n)$ differs from the regular Boltzmann operator because of two terms: the frequency-dependent imaginary $1/v$ absorption cross section appearing on the "disappearance" side of the equation, and the frequency-dependent complex fission multiplicity appearing in the delayed fission operator.

Pioneering work in dealing with these terms within the framework of a Monte Carlo random walk approach has been carried out in reference [33], where the imaginary $1/v$ absorption cross section has been dealt with by modifying the particle weight along each flight. In TRIPOLI-4®, we have chosen instead to work with a real total cross section, and we have thus modified the collision kernel accordingly. This is achieved by following the strategy discussed in [30-31]: we add a term $\eta\omega/v$, η being a real constant and having the same sign as ω, to both sides of the noise equation, and we move the term $i\omega/v$ to the right-hand-side. Then, the noise equation can be identically rewritten as:

$$\left(\mathbf{\Omega}\cdot\nabla + \Sigma_0(\boldsymbol{r}, E) + \eta\frac{\omega}{v}\right)\delta\varphi(\boldsymbol{r}, \mathbf{\Omega}, E, \omega) = \frac{\eta - i}{\eta}\eta\frac{\omega}{v}\delta\varphi(\boldsymbol{r}, \mathbf{\Omega}, E, \omega) + (\dots) \tag{74}$$

Thanks to this algebraic manipulation, we can work with a real modified total cross-section

$$\tilde{\Sigma}_0(\mathbf{r}, E, \omega) = \Sigma_0(\mathbf{r}, E) + \Sigma_\omega(E) > 0 \tag{75}$$

where

$$\Sigma_\omega(E) = \eta\omega/v > 0. \tag{76}$$

Hence, flight lengths are sampled as in standard Monte Carlo calculations, provided that the modified total cross section is used instead of the original unperturbed total cross section. The new term appearing at the right-hand side of the equation can be interpreted as a production operator with a cross section $\eta\omega/v$, a yield $(\eta - i)/\eta$, and a fictitious "delta spectrum" over direction and energy, of the kind $\delta(\mathbf{\Omega} - \mathbf{\Omega}')\delta(E - E')$: in this respect, this term physically represents a *copy operator*.

Because of the structure of the linearized noise equation after the algebraic manipulations above, the collision operator is now composed of two types of particle productions, both appearing on the right-hand side of the transport equation: regular fission with probability $\Sigma_{0,f}/\tilde{\Sigma}_0$, and a special ω-production associated to a *copy operator* with probability $\Sigma_\omega/\tilde{\Sigma}_0$.

We treat fission as customary, i.e., the number of prompt or delayed fission neutrons is determined as $Int(v_q\Sigma_{0,f}/\tilde{\Sigma}_0 + \xi)$, where $Int(...)$ denotes the integer part, ξ is a uniform random number in [0,1), and $q = p,d$. Because of the factor $v^j_{d,\omega}$ appearing in the delayed fission production term, the weight w_d of each new delayed neutron created by fission is modified to:

$$w_d = \frac{w}{k}\left(\frac{\lambda_j^2 - i\lambda_j\omega}{\lambda_j^2 + \omega^2}\right), \tag{77}$$

where w is the particle weight before the fission event. The term representing the ω-production consists of a copy of the incident neutron (energy and direction are the same as before the collision event) with a new weight given by:

$$w_\omega = w\frac{\eta - i}{\eta}. \tag{78}$$

Implicit capture (with forced fission) and Russian roulette can be used as in standard Monte Carlo method. Similar as in [33], Russian roulette is applied separately to the absolute value of the real and imaginary parts of the particle weight: the particle is killed only if the real and the imaginary parts are both killed.

6.3.2 Tallies

Scores such as neutron noise and reaction rates (weighted by the noise) over volumes and space/energy meshes have been extended in order to decompose the complex Monte Carlo estimators into real and imaginary part. If needed, the noise field can be then converted to APSD or CPSD in a post-processing phase, after the calculation.

6.3.3 Convergence and numerical stability

At low and very high frequencies, i.e., far from the plateau region of the zero-power reactor transfer function of the system (typically below 0.01 Hz and above 1 kHz), Monte Carlo methods for noise propagation lead to the production of a very large number of particles and the calculation time explodes [30, 31 and 33]. To perform simulations at low and very high frequencies, a weight cancellation technique has been proposed and tested in [33]; the collision-based method used in TRIPOLI-4® does not use the weight cancellation technique, and nonetheless turns out to be rather robust, with the possible exception of mechanical vibration sources where strong positive/negative particle compensation effects might occur [30, 32]. For more details concerning convergence, we refer the reader to [30].

For the frequency region of interest for most applications in reactor noise analysis, i.e., approximatively between 0.01 Hz and 100 Hz, the TRIPOLI-4® algorithm described above converges safely with $\eta = 1$. Extreme cases beyond this frequency region have also been tested and calculations converge by suppressing implicit capture (and possibly tuning the η value as well at very high frequencies).

To summarize, the TRIPOLI-4® method

(i) uses the conventional algorithm for fixed-source problems for all frequencies,

(ii) does not use the weight cancellation technique, and

(iii) is based on a real total cross-section and a modified collision kernel.

The major advantage of this algorithm is that it introduces minimal modifications to standard Monte Carlo algorithms for particle transport (the key modification concerning the weight modification at delayed fission events and the special “copy” event) and can thus be implemented in continuous-energy production Monte Carlo codes.

6.4 Verification of the TRIPOLI-4® noise solver

The TRIPOLI-4® neutron noise solver developed for CORTEX has been extensively verified, in view of the novelty of its features (in particular the simultaneous presence of real and imaginary particles, each carrying an alternating sign). For this purpose, we have tested the TRIPOLI-4® neutron noise solver against analytical solutions for an infinite homogeneous medium in the case of single-speed and continuous-energy problems, for an infinitely homogeneous cylindrical core, and for one-dimensional homogeneous core surrounded by a reflector. Various kinds of noise sources have been used. All Monte Carlo results (based on the track length estimator) will be plotted with their 1-σ error bars (barely visible in the figures). Other verification tests concerning the basic features of the algorithms had been previously discussed in [30].

6.4.1 Infinite homogeneous medium

For an infinite homogeneous medium in the case of single-speed problem, the results of the TRIPOLI-4® neutron noise solver are verified against analytical results (see [33] for the problem description and the analytical solutions). Here, the noise source is defined by $S = -1 + i$ at each frequency. Results are shown in Figure 4: an excellent agreement is found.

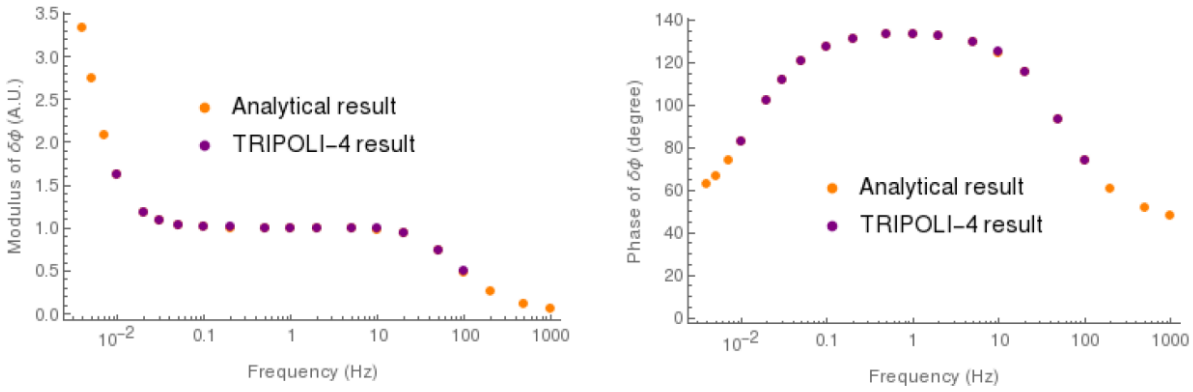

(a) Modulus of the neutron noise. (b) Phase of the neutron noise.

Figure 4: Modulus and phase of the neutron noise versus frequency in an infinite homogeneous medium (single-speed transport).

For an infinite homogeneous medium in the case of continuous-energy problem, the neutron noise solver is again verified against analytical results (see Figure 5). Here, the noise source is defined by $S = 2 - 3i$ between 1 and 2 MeV and $S = 0.75 + 5i$ between 0.0001 and 0.0005 MeV at 3 Hz. For the sake of simplicity, for our tests we have modelled scattering by using a Maxwell spectrum and fission by a Watt spectrum. This example illustrates the capability of the neutron noise solver to correctly simulate continuous-energy problems.

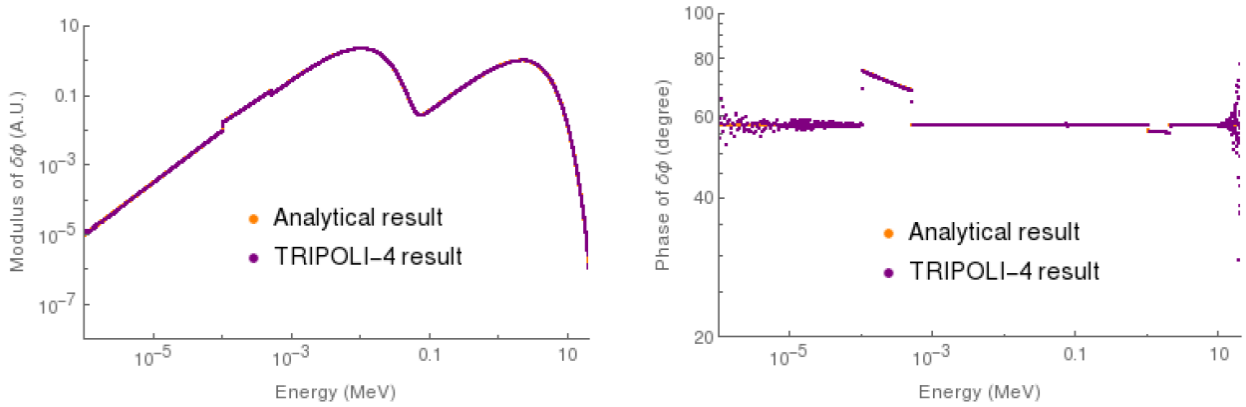

(a) Modulus of the neutron noise. (b) Phase of the neutron noise.

Figure 5: Modulus and phase of the neutron noise versus energy at 3 Hz in an infinite homogeneous medium (continuous-energy transport).

6.4.2 One-dimensional homogeneous core surrounded by a reflector

The final verification test concerns a one-dimensional homogeneous core surrounded by a reflector with two energy groups (see [6] for all details of the problem data and analytical results). Results are shown in Figure 6. Here, the noise source is defined by $S = -3 - 0.5i$ for the fast group and $S = -1.2 + 2i$ for the thermal group at 1Hz and at the core/reflector interface. Again, an excellent agreement is found with respect to exact results.

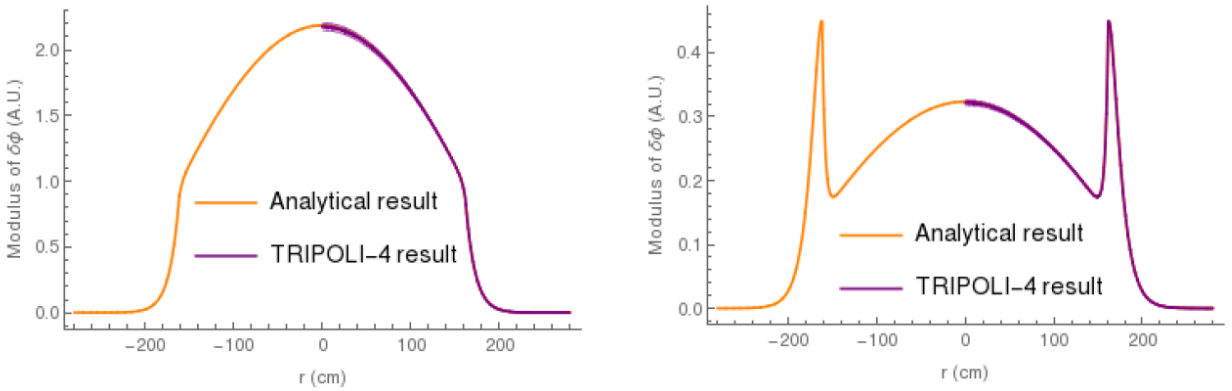

(a) Modulus of the fast neutron noise. (b) Modulus of the thermal neutron noise.

Figure 6: Modulus and phase of the neutron noise versus position at 1 Hz in a one-dimensional homogeneous core surrounded by a reflector.

7 KU Monte Carlo neutron noise solver

A Monte Carlo solver has been developed by Kyoto University (KU) and is used for comparison with other solvers (see section 8.4). The solver allows neutron noise simulations of multi-energy group problems in two- or three-dimensional rectangular geometry. As of now, the number of the energy groups is up to four.

7.1 Neutron noise equation

The fundamental linearized frequency-domain multi-group equation for neutron noise, $\delta\phi_g$, to be solved is a simplified version of Eqs. (4)-(5) and is given by:

$$\boldsymbol{\Omega}\cdot\nabla\delta\phi_g(\boldsymbol{r},\boldsymbol{\Omega},\omega)+\Sigma_{t0g}(\boldsymbol{r})\delta\phi_g(\boldsymbol{r},\boldsymbol{\Omega},\omega)+\frac{1}{4\pi}\sum_{\substack{g'=1\\g\neq g'}}^{G}\Sigma_{s0}^{g\to g'}(\boldsymbol{r})\delta\phi_g(\boldsymbol{r},\boldsymbol{\Omega},\omega)$$

$$=\frac{\chi_g}{4\pi k_{eff}}\left(1-\frac{i\omega\beta}{i\omega+\lambda}\right)\sum_{g'=1}^{G}\nu\Sigma_{f0g'}(\boldsymbol{r})\delta\phi_{g'}(\boldsymbol{r},\boldsymbol{\Omega},\omega)+\frac{1}{4\pi}\sum_{\substack{g'=1\\g\neq g'}}^{G}\Sigma_{s0}^{g'\to g}(\boldsymbol{r})\delta\phi_{g'}(\boldsymbol{r},\boldsymbol{\Omega},\omega)$$

$$-\frac{i\omega}{v_g}\delta\phi_g(\boldsymbol{r},\boldsymbol{\Omega},\omega)+S_g(\boldsymbol{r},\boldsymbol{\Omega},\omega) \tag{79}$$

where ω is the angular frequency of the neutron noise; the subscript 0 denotes an unperturbed parameter; other notations are standard in the nuclear engineering field. Here, the macroscopic scattering cross section is isotropic and one delayed neutron group is assumed. The Monte Carlo algorithm for solving this equation is almost the same as for ordinary neutron transport calculations. The main differences are that the flux for neutron noise has two values (i.e., real and complex values); the fission neutron is multiplied by $(1-i\omega\beta/(i\omega+\lambda))$ as seen in the first term on the right-hand side; the third term on the right-hand side needs to be included during the random walk process; and the last term is the neutron noise source.

7.2 Monte Carlo solution algorithm

The Monte Carlo procedure for the solution of Eq. (79), the estimators used for neutron noise, the applicability with respect to the frequency range, and the use of neutron cross sections and model geometry from the code SIMULATE-5 are discussed.

7.2.1 Procedures of Monte Carlo calculation by KU

The Monte Carlo calculation flow for solving the neutron noise transport equation is presented here as follows [33]:

(1) A noise source particle is emitted from the neutron noise source position. The position, direction, and energy group of the noise source in the frequency domain is determined according to $S_g(\boldsymbol{r},\boldsymbol{\Omega},\omega)$. The particle weight is usually a complex value.
(2) The particle is transported to the collision point that is determined by the same procedure as the ordinary Monte Carlo transport calculations.
(3) However, we need to consider the third term on the right-hand side of Eq. (79). There exist several methods for considering this term. The KU solver adopts a method where the particle weight continuously changes as follows:

$$W_{j+1}=W_j\cdot exp\left(-\frac{i\omega}{v_{gj}}s_j\right), \tag{80}$$

where W_j is the particle weight at the beginning of the *j*-th flight path whose flight length is s_j; W_{j+1} is the weight at the end of the flight.
(4) At each collision point, weight reduction is performed as in the ordinary Monte Carlo method. The weights of the real and imaginary parts are multiplied by Σ_s/Σ_t.
(5) Russian roulette game is played if either of the real or imaginary part of the complex-valued weight is below the lower weight boundary for Russian roulette game. If both the real and imaginary parts are killed at the same time, the particle is killed. However, if one of both parts survives, the particle still continues to fly.
(6) If fission reaction occurs at a collision point, particles caused by the fission reaction are generated as the ordinary Monte Carlo transport calculations. However, the weights of the particles are multiplied by $(1-i\omega\beta/(i\omega+\lambda))$.
(7) After the particle emitted from the source and its progenies are killed, return to step (1) and a new source particle is emitted.
(8) Repeat steps (1) through (7) until desired statistics are obtained.

7.2.2 Tallying

During the random walk process presented in section 7.1.1, the neutron noise is calculated using the collision estimator or the track length estimators. The collision estimator accumulates the estimates w/Σ_{tg} at each collision point where w is a complex-valued weight and thus the estimate is also a complex value. The track length estimator is different from the ordinary Monte Carlo transport calculations because the weight changes continuously during the flight. The track length estimator for the *j*-th flight path is given by

$$TL_j = \int_0^{s_j} W_j \cdot exp\left(-\frac{i\omega}{v_{gj}}s'\right) ds' = W_j \frac{iv_{gj}}{\omega}\left(exp\left(-\frac{i\omega}{v_{gj}}s_j\right) - 1\right). \quad (81)$$

7.2.3 Available frequency range

As pointed out in [30, 33], too many particles are produced when we solve Eq. (79) for frequency range outside the plateau frequency range, thereby resulting in abnormal termination of the Monte Carlo calculation. A Monte Carlo algorithm to circumvent this difficulty is proposed in [30, 33]. However, implementing such an elaborate algorithm is omitted in the solver developed here. Thus, the frequency range where the solver is applicable is limited, i.e., approximately between 0.05 and 30 Hz.

7.2.4 Connection with SIMULATE-5

The Monte Carlo solver has a capability of reading macroscopic cross sections and core geometry from the output file of the code SIMULATE-5 [34]. The Monte Carlo solver can automatically construct the same 3D core configuration as in SIMULATE-5. While SIMULATE-5 uses diffusion coefficients, the total cross sections that the Monte Carlo solver uses is approximated by $\Sigma_t \approx 1/(3D)$ and isotropic scattering is assumed. The discontinuity factors in SIMULATE-5 are used in the Monte Carlo solver when a particle passes through a boundary between node 1 and node 2 as

$$W_2 = W_1 \cdot \frac{DF_1}{DF_2}, \quad (82)$$

where W_1 and W_2 are the particle weights on the boundary surface between node 1 and node 2, respectively and DF_1 and DF_2 are the discontinuity factors on the boundary surface between node 1 and node 2, respectively.

8 Comparisons of neutron noise solvers

The solvers discussed above have been compared to verify their algorithms. In addition, comparisons have also been carried out between these solvers and diffusion-based solvers to investigate possible differences between higher-order and low-order methods.

8.1 Comparison between TRIPOLI-4® and APOLLO3®

In order to illustrate the capabilities and the accuracy of the APOLLO3® and TRIPOLI-4® neutron noise solvers, we have performed code-to-code comparisons for two neutron noise simulations in a simplified UOX fuel assembly, in two dimensions. In this section, we describe the examined geometry and material compositions, and then the neutron noise simulations: the neutron noise induced by a simple isotropic noise source and by a cross-section oscillation.

8.1.1 Description of the test configuration

The chosen geometry is a simplified UOX fuel assembly, with reflecting boundary conditions, composed by 264 homogeneous square fuel pins y (0.7314 x 0.7314 cm) with 25 homogeneous water holes (1.26 x 1.26 cm). The square configuration of the fuel pins is required by the 2-D neutron noise solver developed in APOLLO3® being restricted to homogeneous Cartesian geometries for

the time being. For the sake of simplicity, and in view of comparing the two solvers on clean configurations where a high numerical accuracy can be achieved, all simulations (steady state and noise transport) have been performed with two energy groups (fast and thermal groups without up-scattering) and one precursors family. For the APOLLO3® transport solver, we chose an order of discrete ordinates S32 and a constant approximation of the volume flux with the spatial meshes, as shown in Figure 7.

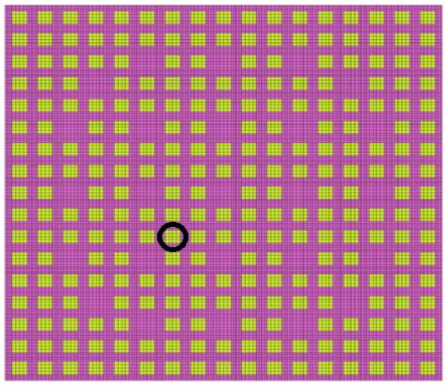

Figure 7: Simplified UOX fuel assembly: 2D geometry with spatial meshes. The perturbed fuel pin is marked in black.

For the criticality calculations, we obtain a critical k-eigenvalue equal to 0.99912 ± 8x10^{-5} with TRIPOLI-4® (with 3x10^{4} active cycles and 10^{4} neutrons per cycle) and to 0.99784 with APOLLO3® (10^{-6} tolerance on the outer iterations and no acceleration). The corresponding steady-state fluxes are shown in Figure 8. Relative errors between APOLLO3® and TRIPOLI-4® for the steady-state fluxes are smaller than 1% on the whole assembly.

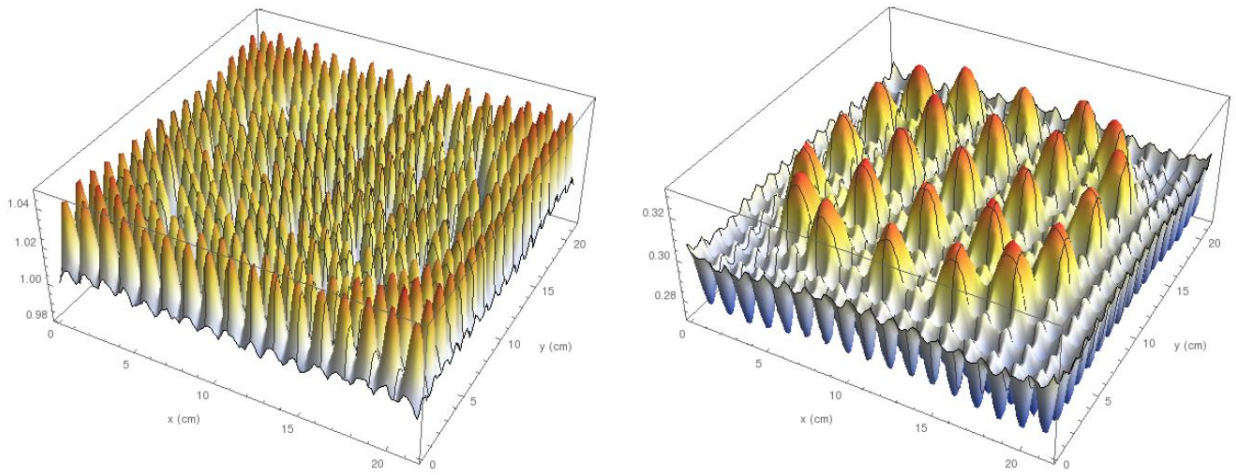

(a) Fast group (A.U.). (b) Thermal group (A.U.).

Figure 8: Steady-state flux of the reference case (scalar flux, TRIPOLI-4® results with $\sigma < 0.3\%$).

8.1.2 A simple noise source

As a first noise calculation for the two solvers, we impose a simple isotropic noise source $S = -1 + i$ at ω = 3 Hz in a perturbed fuel pin, in the thermal group (the location of the perturbed fuel pin is detailed in the figure of the assembly geometry above). Simulation findings for the spatially and energy-resolved over the fuel assembly are shown in Figure 9 (we have converted the real and imaginary part in polar form, with modulus and phase). The phase of the neutron noise is almost

constant and is not shown here. The noise calculations of TRIPOLI-4® have been performed with $3x10^3$ replicas and 10^4 particles per replica.

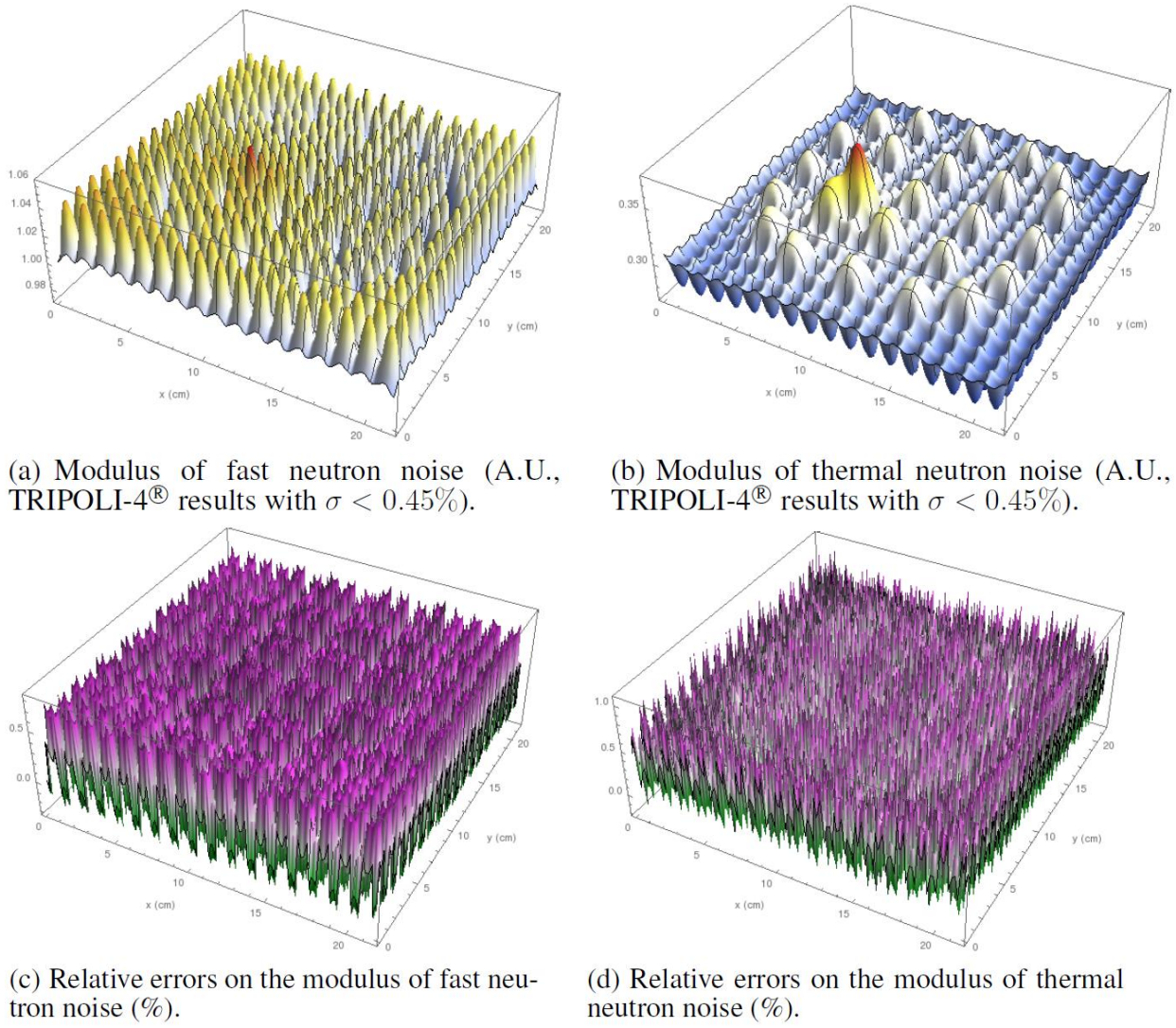

(a) Modulus of fast neutron noise (A.U., TRIPOLI-4® results with $\sigma < 0.45\%$).

(b) Modulus of thermal neutron noise (A.U., TRIPOLI-4® results with $\sigma < 0.45\%$).

(c) Relative errors on the modulus of fast neutron noise (%).

(d) Relative errors on the modulus of thermal neutron noise (%).

Figure 9: Results and relative errors (%) between TRIPOLI-4® and APOLLO3® on the modulus of the noise field $\delta\Psi$ induced by a simple isotropic noise source at $\omega = 3$ Hz.

A good agreement is found between APOLLO3® and TRIPOLI-4®: the relative errors on the modulus are comparable to the relative errors on the steady-state flux, i.e., smaller than 1% over the assembly.

8.1.3 An oscillation-induced noise source

We consider next the spatially and energy-resolved modulus and phase of the noise field $\delta\Psi$ induced by a sinusoidal oscillation of all macroscopic cross-sections of a perturbed fuel pin at ω = 1 Hz (the position of the perturbed fuel pin is detailed in the figure of the assembly geometry above). The perturbed cross section term in the time domain is defined by:

$$\delta\Sigma(r, E, t) \;=\; \rho\Sigma_0(r, E)\cos(\omega_0 t) \tag{83}$$

with ω_0 the angular frequency of the perturbation (here $\omega_0 = 2\pi$ rad/s). The perturbation amplitude is taken as ρ = 4.1% for the total cross-section, ρ = 3.4% for the scattering cross-section and ρ = 2.1% for the fission cross-section. Results are shown in Figure 10 for a noise source corresponding to a

critical state Ψ_0 computed as detailed above. The phase of the neutron noise is again almost constant and will not be shown. The noise calculations of TRIPOLI-4® have been performed with 10^5 replicas and 3 x 10^4 particles per replica.

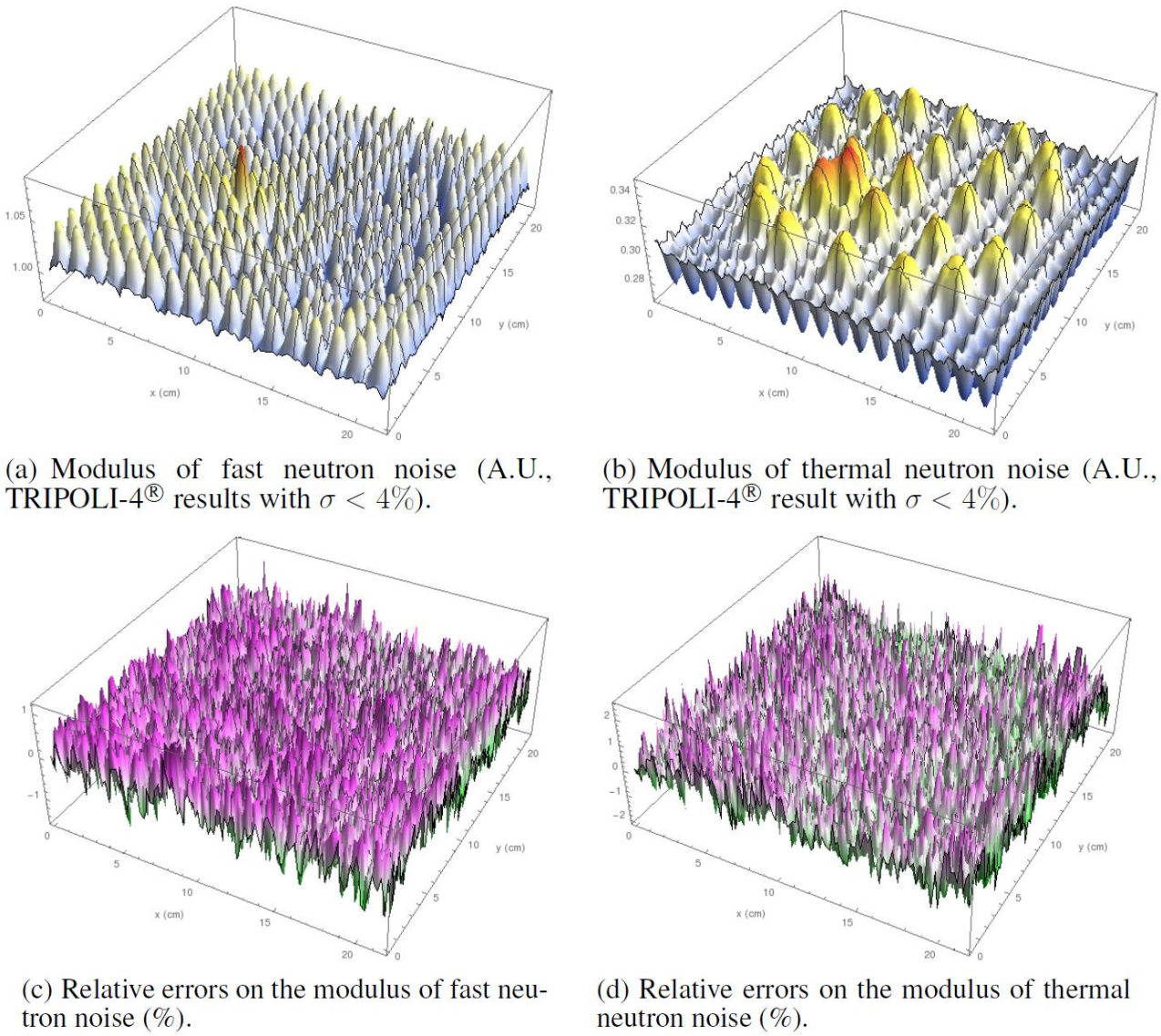

(a) Modulus of fast neutron noise (A.U., TRIPOLI-4® results with $\sigma < 4\%$).

(b) Modulus of thermal neutron noise (A.U., TRIPOLI-4® result with $\sigma < 4\%$).

(c) Relative errors on the modulus of fast neutron noise (%).

(d) Relative errors on the modulus of thermal neutron noise (%).

Figure 10: Results and relative errors (%) between TRIPOLI-4® and APOLLO3® on the modulus of the noise field $\delta\Psi$ induced by an oscillation noise source at $\omega = 1$ Hz.

Similarly, as for the previous case, a good agreement is found between APOLLO3® and TRIPOLI-4® for the oscillation calculation: the relative errors on the modulus are smaller than 2%.

8.2 Comparison between NOISE-SN and CORE SIM

An initial version of the neutron noise solver NOISE-SN has been compared with CORE SIM, which is a solver based on diffusion theory [6]. For the comparison, a two-dimensional, heterogeneous critical system with a localized perturbation, is considered. More details of this work are discussed in [35].

8.2.1 Neutron noise problem based on the C3 system

A neutron noise problem in a 2-D heterogeneous system is considered. The system is based on the C3 benchmark on deterministic transport calculations [36] and it is perturbed by introducing a

localized neutron noise source. The system configuration is given in Figure 11. It consists of two UO2 fuel assemblies (at North-West and South-East positions) and two MOX fuel assemblies (at North-East and South-West positions). The dark blue squares in the illustration are guide tubes; the ones in the center of the fuel assemblies contain fission chambers. Reflective boundary conditions are imposed. The perturbation is a fluctuation of 5% of the fast and thermal neutron capture cross-sections in the fuel cell (16,19) identified with a red square in Figure 11.

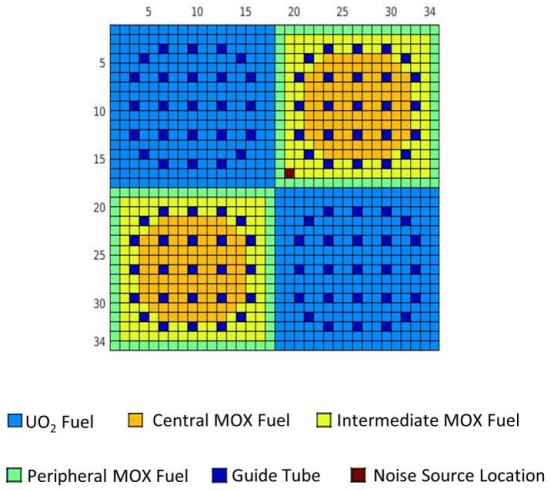

Figure 11: C3 configuration and location of the neutron noise source (in red).

8.2.2 Results

The effect of the frequency of the neutron noise source, is investigated with respect to the range between 0.01 Hz and 100 Hz. The resolution of the spatial mesh is chosen to be 5x5 nodes per fuel cell/guide tube, and the S_8 approximation is used for the discrete ordinate solver. The results for the neutron noise amplitude are presented in Figures 12 to 15 and they are respectively related to the following locations: (16,19) where the perturbation is placed; (17,18) as representative of fuel cells close to the perturbation; (25,10) as representative of the fuel cells far away from the perturbation; (31,4) as representative of the guide tubes in the MOX fuel assemblies. In addition, Figures 16 and 17 provide an example of the behavior of the phase of the neutron noise, taken respectively at the location of the perturbation (16,19) and at the location (17,18) close to the perturbation.

In general, the behavior of the predicted neutron noise with respect to the frequency is consistent with the theoretical zero-power reactor transfer function. Accordingly, at low and high frequencies the neutron noise amplitude decreases with the increase of frequency, while at intermediate frequencies a plateau region can be identified where the neutron noise amplitude is approximately constant. The neutron noise phase resembles a bell-shaped curve, and it is also approximately constant at intermediate frequencies. The discrepancies between CORE SIM and the discrete ordinates solver change over the frequency range, although they are nearly insensitive in the plateau region.

The discrepancies of the neutron noise amplitudes calculated with the 2 solvers at the location of the perturbation and at locations close to the perturbation, are relatively large and increase with frequency (see Figures 12 and 13). In particular, at the location of the neutron noise source, the relative differences for the fast amplitude vary from ~ -4% to ~ -11% over the frequency range, and the ones for the thermal amplitude vary from ~ -8% to ~ -24%. Since a strong gradient of the neutron flux occurs near the perturbation, a higher-order transport method may reproduce the phenomenon better than a diffusion-based model. In addition, the differences may be more notable at higher frequencies for which the propagating effect of the disturbance needs to follow faster fluctuations of the system properties.

The discrepancies between CORE SIM and the discrete ordinates solver at locations of fuel cells far away from the perturbation, are relatively small and quite insensitive to frequency. For position

(25,10), the relative differences of the amplitude are below 1% for the fast group, and around 1.2 – 1.6% for the thermal group (see Figure 14). Considering the highly localized effect of the perturbation, these discrepancies are mainly due to differences in the static calculations, which are not dependent on the frequency of the neutron noise source.

When considering the neutron noise in the guide tubes, discrepancies between CORE SIM and the discrete ordinates solver are significant, but they are only weakly affected by the frequency of the neutron noise source. As shown in Figure 15, the relative differences in the guide tube (31,4) reach ~12%. These large values are mainly related to the large discrepancies already existing in the static neutron flux because of the sharp heterogeneity introduced with the guide tubes, and thus are nearly independent from the frequency.

The discrepancies between the neutron noise phases evaluated with CORE SIM and with the discrete ordinates solver are relatively small and constant in the plateau region. For this interval of frequencies, a phase close to 180 degrees is expected because the perturbation of the macroscopic neutron capture cross-section induces an out-of-phase response of the neutron flux. Outside the plateau region, the relative differences may be somewhat larger. At the location of the perturbation, they are found to be (see Figure 16): ~ -1% for the fast neutron noise and ~ -3% for the thermal neutron noise at the frequency of 0.01 Hz; and ~ -6% for the fast neutron noise and ~ -3.5% for the thermal neutron noise at the frequency of 100 Hz. When taking other locations, CORE SIM and the discrete ordinates solver provide very similar results. For example, the relative differences are approximately below 1.2% already in the fuel cell (17,18) which is just next to the perturbed one (see Figure 17).

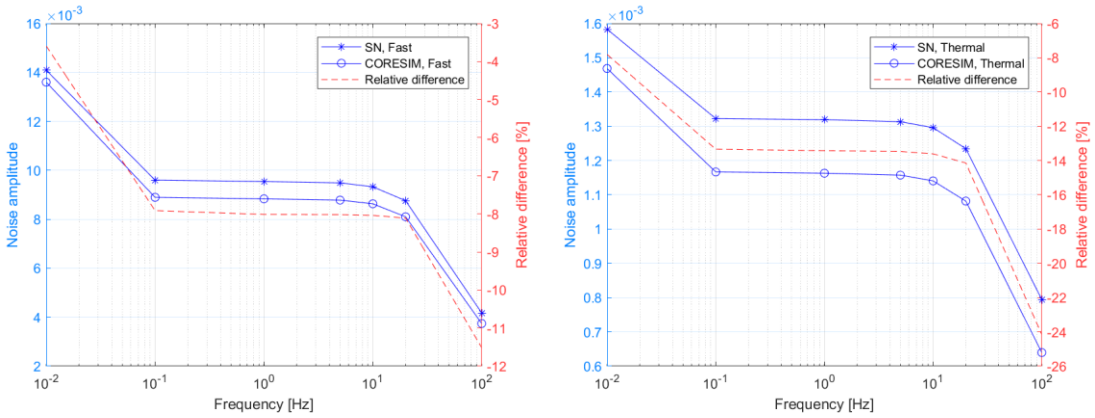

Figure 12: Relative differences between the 2 solvers at the location of the neutron noise source, for the amplitude of the fast (left) and thermal (right) neutron noise.

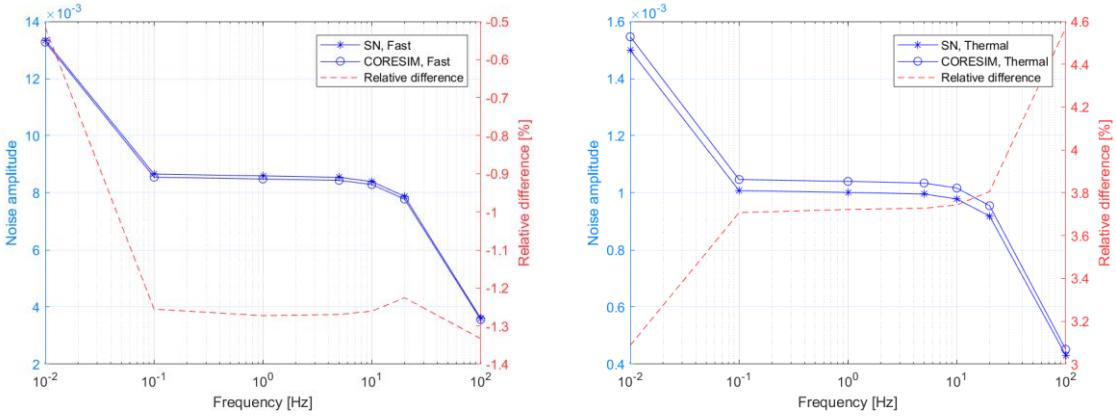

Figure 13: Relative differences between the 2 solvers at the location (17,18), for the amplitude of the fast (left) and thermal (right) neutron noise.

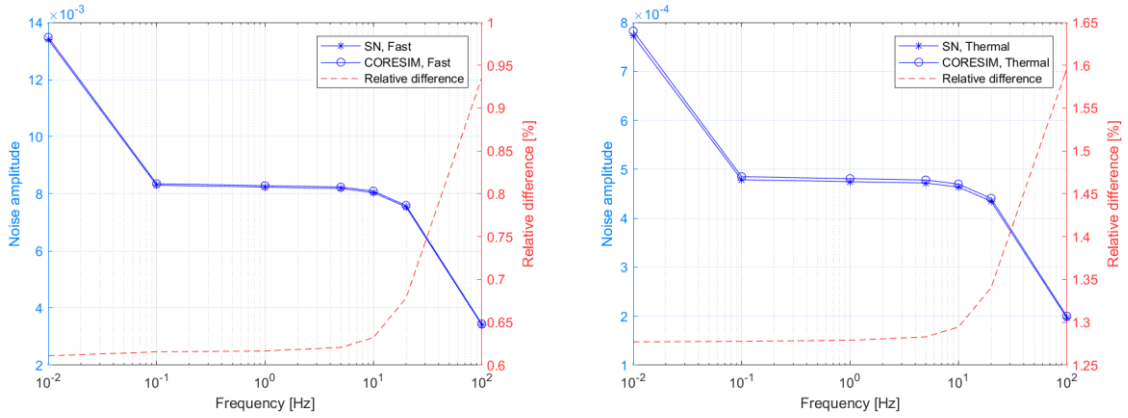

Figure 14: Relative differences between the 2 solvers at the location (25,10), for the amplitude of the fast (left) and thermal (right) neutron noise.

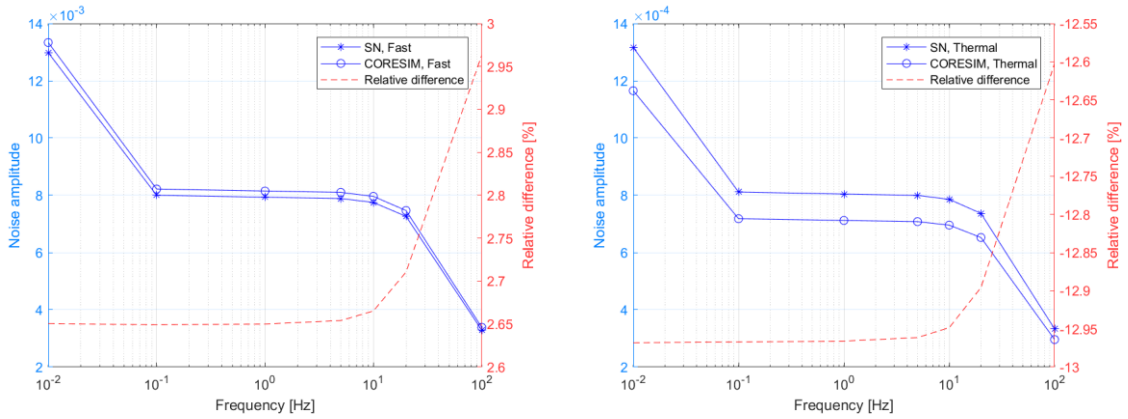

Figure 15: Relative differences between the 2 solvers at the location (31,4), for the amplitude of the fast (left) and thermal (right) neutron noise.

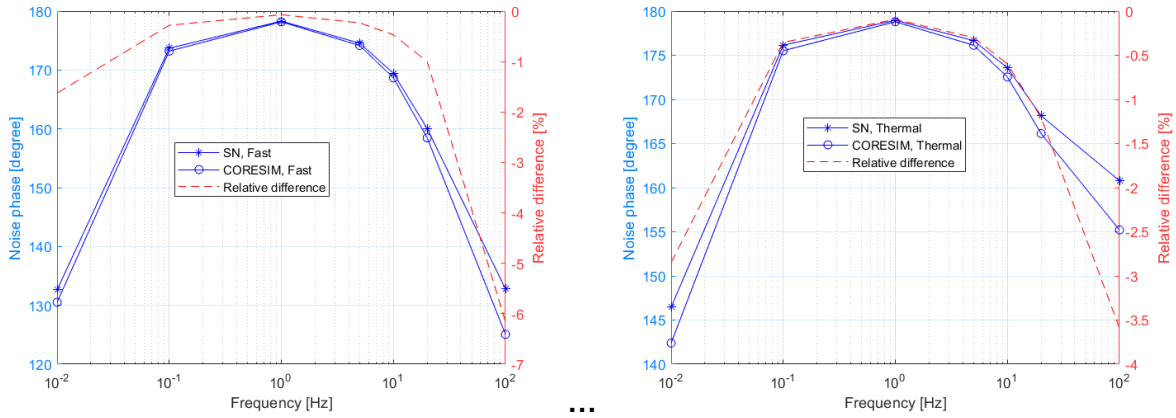

...

Figure 16: Relative differences between the 2 solvers at the location of the neutron noise source, for the phase of the fast (left) and thermal (right) neutron noise.

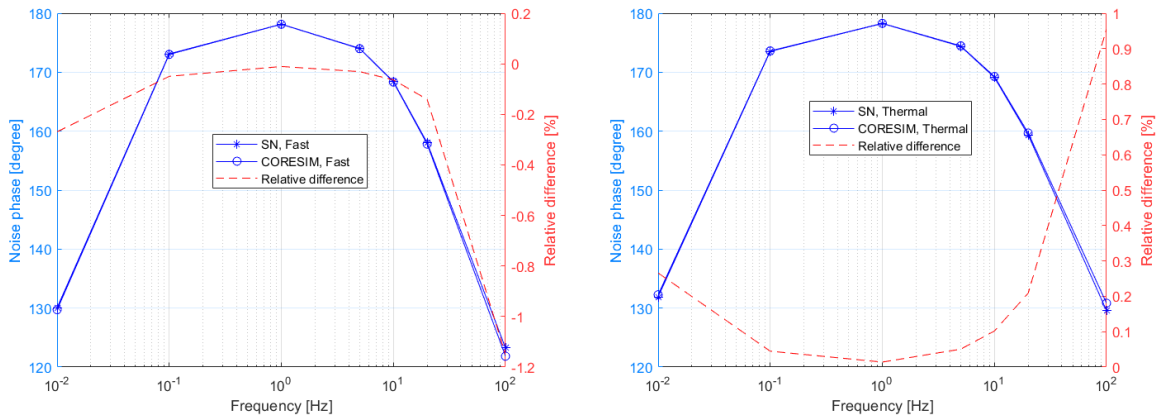

Figure 17: Relative differences between the 2 solvers at the location (17,18), for the phase of the fast (left) and thermal (right) neutron noise.

8.3 Comparison of the Chalmers Monte Carlo-based method with CORE SIM

Two problems have been used to compare the Monte Carlo-based method discussed in section 5 with the deterministic neutron noise diffusion solver CORE SIM [6]. The first problem is based on a homogeneous system and the second problem consists of a heterogeneous system.

8.3.1 Homogeneous test case

A one-dimensional slab of thickness 201 cm is considered, with vacuum boundary conditions applied. The static macroscopic cross-sections, point-kinetic data, and noise source definition are given in [20]. The neutron noise source is placed in the middle of the slab and consists of a perturbation of all the neutron cross sections, with a frequency of 0.0135 Hz. The choice of the frequency is such that both the real and imaginary parts of the noise are relevant.

Figure 18 shows that the induced neutron noise predicted with the Monte Carlo-based method agrees very well with the CORE SIM solution. The local component of the neutron noise is particularly well reproduced. Some small deviation in the prediction of the global component can nevertheless be noticed, where the “buckling” of the amplitude of the global component is slightly different between the two solutions and where the slope of the phase of the global component also slightly differs in the thermal group. The maximum relative difference in amplitude is $\sim 10\%$, whereas the maximum difference in phase is ~ 2 deg.

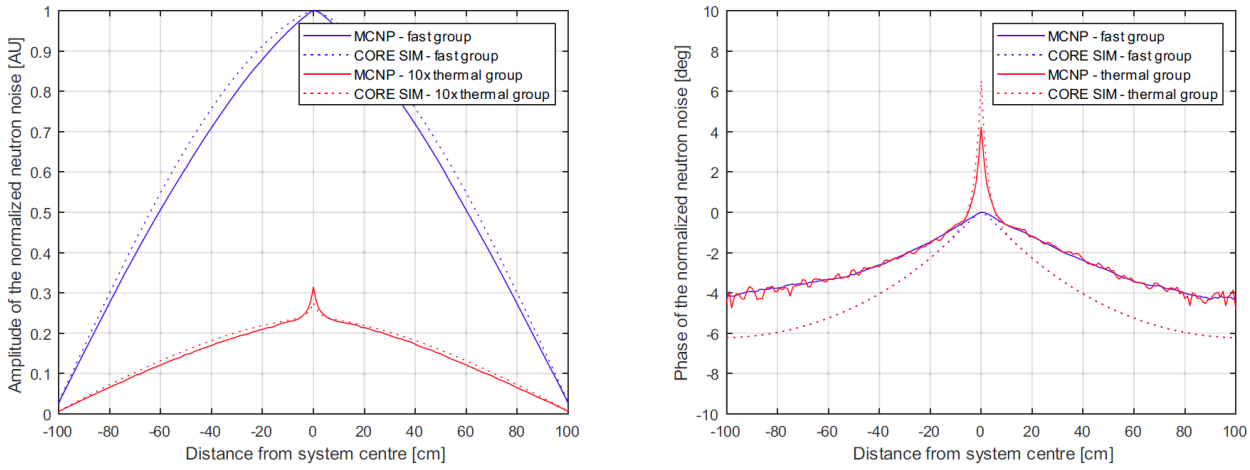

Figure 18: Results for the homogeneous test case. All results were normalized to the same induced neutron noise in the fast energy group at the location of the noise source.

8.3.2 Heterogeneous test case

A one-dimensional system made of 11 fuel pins, each pin being of 1 cm thickness surrounded by water, is defined, with vacuum boundary conditions applied. The spacing between each fuel pin is 0.25 cm, whereas the spacing between the outer periphery of the outermost fuel pins and the boundary of the system is 0.125 cm. The static macroscopic cross-sections, point-kinetic data, and noise source definition are given in [20]. Again, the neutron noise source is placed in the middle of the slab and consists of a perturbation of all the macroscopic cross sections, with a frequency of 0.159 Hz.

As shown in Figure 19, the amplitude and the phase calculated with CORE SIM are reproduced by the Monte Carlo-based method. However, the Monte Carlo transport solution has a larger spatial variation on small scales, as compared to the diffusion-based CORE SIM solution. As for the homogeneous case, a slightly different slope in the phase of the induced thermal neutron noise is observed. The variation of the phase throughout the system is less than 0.6 deg and thus the observed differences may be considered negligible.

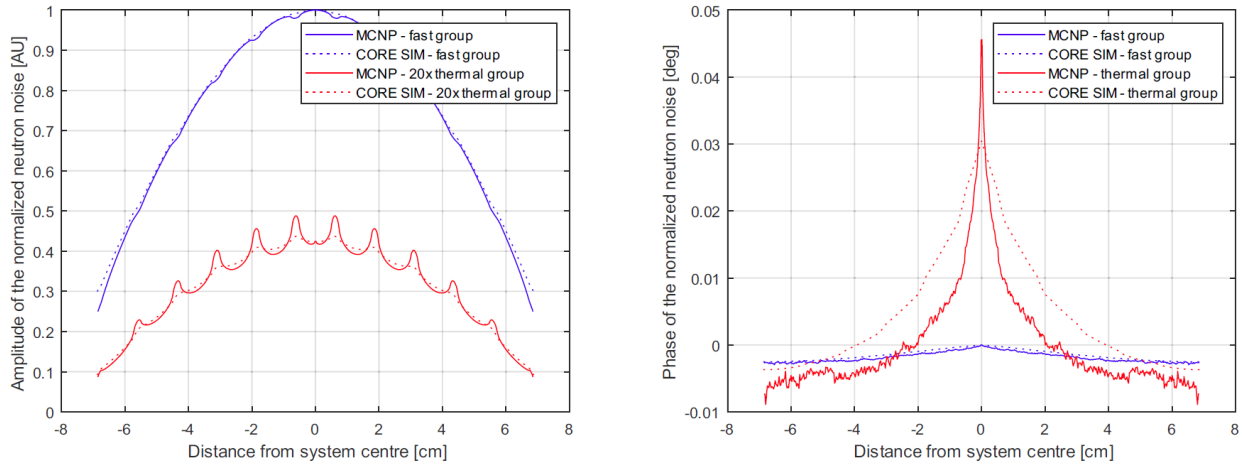

Figure 19: Results for the heterogeneous test case. All results were normalized to the same induced neutron noise in the fast energy group at the location of the noise source.

8.4 Comparison between neutron noise solvers using numerical benchmarks in a 2-D simplified UOX fuel assembly

Neutron noise solvers developed in the CORTEX project have been compared using two neutron noise benchmarks. In the current section, these benchmarks are respectively referred to as exercise 1 (simple noise source, see subsection 8.1.2) and exercise 2 (oscillating noise source, see subsection 8.1.2). The system is a simplified UOX fuel assembly whose nuclear data are generated with respect to 2 energy groups, and scattering is assumed to be isotropic. All the solvers, including the Monte Carlo ones, use the same set of pre-generated cross sections.

The solvers used for the simulation of the 2 exercises are: the frequency-domain stochastic neutron noise solver in TRIPOLI-4® (section 6), the frequency-domain Monte Carlo neutron noise solver developed by Kyoto University (section 7), the frequency-domain deterministic solver NOISE-SN (the SN solver developed by Chalmers, section 2), the frequency-domain deterministic IDT lattice solver in APOLLO3® (section 3), the frequency-domain neutron noise diffusion solver CORE SIM+ [7, 37], and the time-domain finite-element diffusion solver FEMFFUSION [7, 38, 39].

The quantities chosen for the comparison of the solvers are the neutron flux and the multiplication factor in the static configuration without perturbations, and the relative amplitude and phase of the neutron noise calculated in the two exercises. For illustration, the results for the thermal energy group

are taken along the main diagonal of the fuel assembly that crosses the perturbed fuel pin. The TRIPOLI-4® simulations are selected as the reference. The detailed discussion of the analysis can be found in [40].

8.4.1 Static neutron flux

The calculated values of the multiplication factor of the static configuration are summarized in Table 1. The KU Monte Carlo solver, the IDT solver embedded in APOLLO3®, and NOISE-SN predict values close to the multiplication factor obtained from TRIPOLI-4®. The diffusion-based codes CORE SIM+ and FEMFFUSION exceed the reference by more than 1000 pcm. The thermal static neutron flux and the relative differences between the solvers and TRIPOLI-4® are shown in Figure 20. The relative differences associated with the KU Monte Carlo solver and with the deterministic higher-order transport methods are between ± ~1%. The relative differences associated with the diffusion solvers are between +2% and -6% for the thermal neutron flux. The larger discrepancies between the diffusion and Monte Carlo calculations are found in the water holes and in the middle of the moderator regions between the fuel pins. Although not included in the plots, the standard deviations associated with the Monte Carlo results are sufficiently small to ensure the accurate estimation of the neutron fluxes.

Table 1: Multiplication factor, comparison between solvers over the static configuration.

Solvers	k_{eff}	Difference [pcm]
TRIPOLI-4®	0.99912 ± 8 pcm	Reference
KU Monte Carlo solver	0.99919 ± 7 pcm	7
APOLLO-3®	0.99784	-128
NOISE-SN	0.99996	84
CORE SIM+	1.01309	1397
FEMFFUSION	1.01367	1485

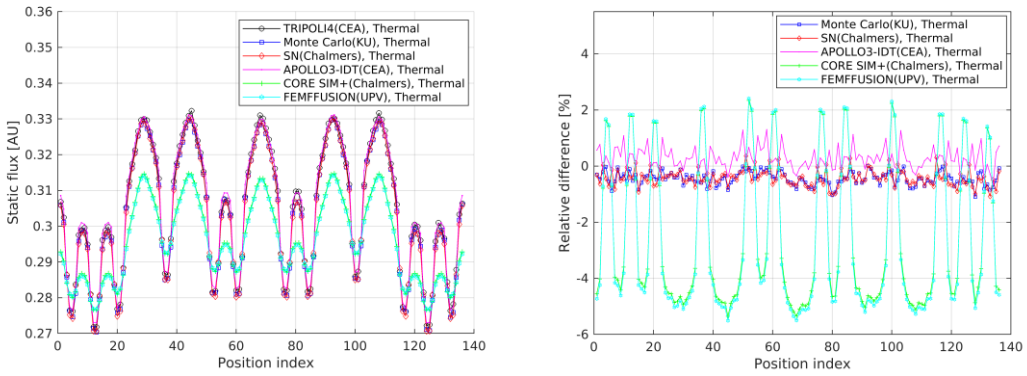

Figure 20: Thermal static flux (left) and relative differences with respect to TRIPOLI-4® (right), along the main diagonal of the fuel assembly crossing the perturbed fuel pin.

8.4.2 Neutron noise

For the neutron noise calculated in the two exercises, the Monte Carlo solver developed by Kyoto University, the IDT solver embedded in APOLLO3®, and NOISE-SN are in good agreement with TRIPOLI-4®. The differences estimated with respect to TRIPOLI-4® are between ±2% for the relative noise amplitude of the thermal group (see Figures 21 for exercise 1 and Figure 22 for exercise 2).

For the diffusion-based solvers, the largest discrepancies are found close to the neutron noise source, where the diffusion approximation is expected to be less reliable. In exercise 1, the maximum relative differences between CORE SIM+ and TRIPOLI-4® are about -9% for the relative thermal noise amplitude (see Figure 21). In exercise 2, the biggest relative differences between CORE SIM+ and TRIPOLI-4® are about -8% for the relative thermal noise amplitude (see Figure 22). The solver FEMFFUSION is used only in the second exercise and its relative differences with TRIPOLI-4® can reach about -13% in the thermal group (see Figure 22). Far from the noise source, the diffusion calculations are consistent with the results of the higher-order transport methods.

All the solvers predict very similar values for the phase of the noise. For example, the case of exercise 2 is considered; the thermal noise phase is shown in Figure 23. The relative differences with respect to TRIPOLI-4® are between ±0.15% for all the frequency-domain solvers. FEMFFUSION gives values with a slight shift (around -0.25%).

In the Monte Carlo simulations, uncertainties for the real and imaginary parts of the neutron noise are estimated separately via independent replicas. Because of the non-linear and highly correlated transformations required, a precise uncertainty for the amplitude and the phase cannot be assessed. However, in view of the high degree of statistical convergence on the real and imaginary parts, the results provided for the amplitude and phase are assumed to be sound and reliable.

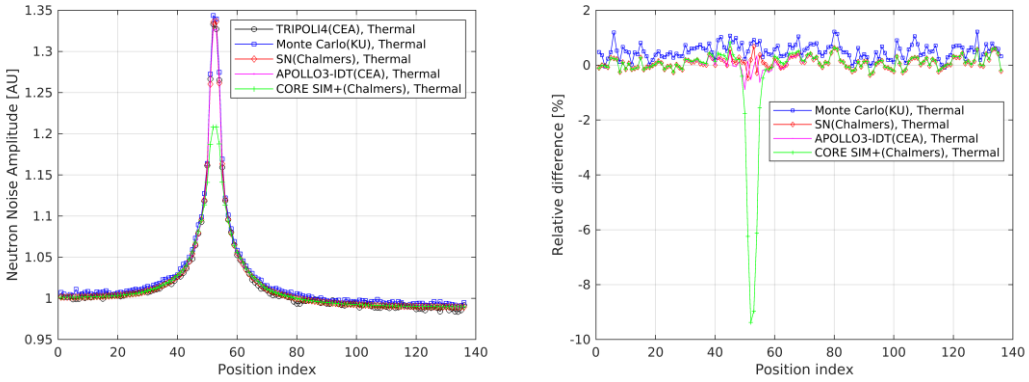

Figure 21: Exercise 1; relative thermal noise amplitude (left) and relative differences with respect to TRIPOLI-4® (right), along the main diagonal of the fuel assembly crossing the perturbed fuel pin.

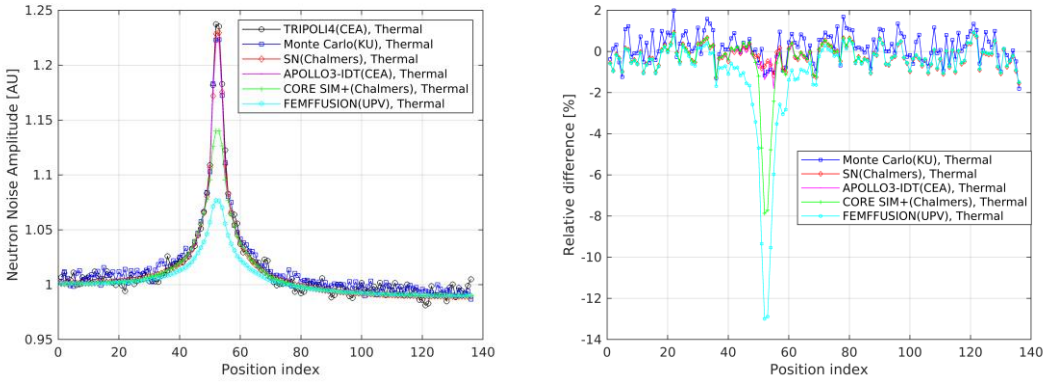

Figure 22: Exercise 2; relative thermal noise amplitude (left) and relative differences with respect to TRIPOLI-4® (right), along the main diagonal of the fuel assembly crossing the perturbed fuel pin.

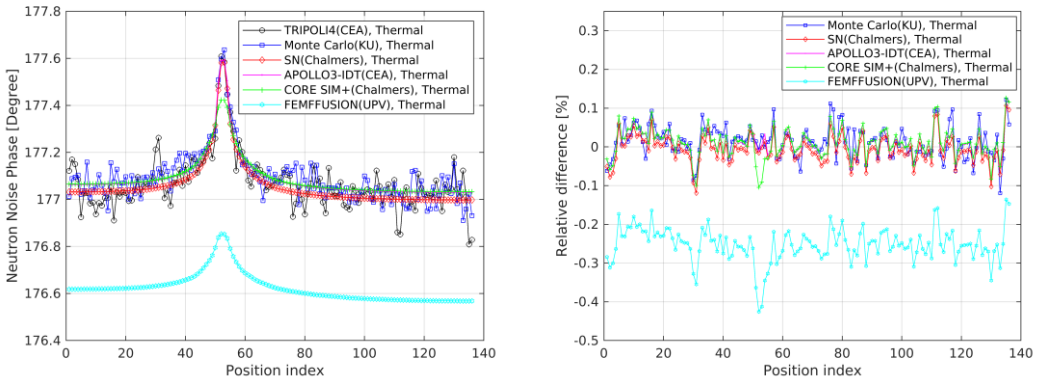

Figure 23: Exercise 2; thermal noise phase (left) and relative differences with respect to TRIPOLI-4® (right), along the main diagonal of the fuel assembly crossing the perturbed fuel pin.

9 Conclusions

In the CORTEX project, Monte Carlo and deterministic higher-order transport methods have been used to develop solvers and procedures for neutron noise simulations, i.e.:

- The deterministic solver NOISE-SN, using a discrete ordinates method (Chalmers University of Technology)
- The deterministic IDT lattice solver embedded in APOLLO3® for frequency-domain calculations (CEA)
- The deterministic APOLLO3® IPK solver for time-domain calculations (CEA)
- A stochastic solver in the Monte Carlo code TRIPOLI-4® for frequency-domain calculations (CEA)
- A procedure for frequency-domain calculations using a stochastic code (Chalmers University of Technology)
- A Monte Carlo solver for frequency-domain calculations (Kyoto University)

These solvers have been applied to various numerical neutron noise problems in which localized fluctuations of macroscopic neutron cross sections are prescribed. The comparisons between them show similar results and the correct implementation of the algorithms.

In the comparisons between the stochastic solvers, the higher-order deterministic solvers, and the diffusion-based solvers such as CORE SIM+ and FEMFFUSION, a relatively good agreement is found, although diffusion theory may be less accurate close to the neutron noise sources and in regions characterized by strong variation of the material properties.

Further work will be necessary to test the solvers when simulating neutron noise induced by mechanical vibrations.

10 References

[1] C. Demazière, P. Vinai, M. Hursin, S. Kollias and J. Herb, “Overview of the CORTEX project,” in Proc. Int. Conf. Physics of Reactors− Reactor Physics paving the way towards more efficient systems (PHYSOR2018), Cancun, Mexico, (April 2018).

[2] P. Stulik et al., CORTEX D3.3: Development of advanced signal processing techniques and evaluation results, 2019.

[3] S. Kollias et al., CORTEX D3.4: Development of machine learning techniques and evaluation of analysis results, 2019.

[4] G. Alexandridis et al., CORTEX D4.4: Results of the application and demonstration calculations, 2020.

[5] I. Pázsit, “Dynamic transfer function calculations for core diagnostics”, Annals of Nuclear Energy, 19(5), May 1992, pp. 303-312 (1992).

[6] C. Demazière, “CORE SIM: A Multi-purpose Neutronic Tool for Research and Education,” Annals of Nuclear Energy, 38(12), December 2011, pp. 2698-2718 (2011

[7] A. Vidal-Ferràndiz et al., CORTEX D1.3: Modelling of the neutron flux response to vibrating fuel assemblies, 2020.

[8] H. Yi, P. Vinai and C. Demazière, “A discrete ordinates solver with diffusion synthetic acceleration for simulations of 2-D and 2-energy group neutron noise problems,” The International Conference M&C-2019, pp. 2023–2032 (2019).

[9] H. Yi, P. Vinai and C. Demazière, “Acceleration of a 2-Dimensional, 2-Energy-Group Neutron Noise Solver Based on a Discrete Ordinates Method in The Frequency Domain,” International Conference PHYSOR-2020, EPJ Web of Conferences, 247, 21005 (2021).

[10] H. Yi, P. Vinai and C. Demazière, “On neutron noise simulations using the discrete ordinates method,” submitted to Annals of Nuclear Energy (2021).

[11] E. E. Lewis & W.F. Miller, “Computational methods of neutron transport,” (1984).

[12] G. Longoni, “Advanced quadrature sets and acceleration and preconditioning techniques for the discrete ordinates method in parallel computing environments,” PhD thesis, University of Florida: Gainesville, FL (2004).

[13] D.G. Cacuci, “Handbook of Nuclear Engineering: Vol. 2: Reactor Design,” Springer Science & Business Media (2010).

[14] M. Jarrett, B. Kochunas, A. Zhu and T. Downar, “Analysis of stabilization techniques for CMFD acceleration of neutron transport problems,” Nuclear Science and Engineering, 184(2), pp. 208-227 (2016).

[15] K.D. Lathrop, “Remedies for ray effects,” Nuclear Science and Engineering, 45(3), pp. 255-268 (1971).

[16] W. F. Miller Jr & W.H. Reed, “Ray-effect mitigation methods for two-dimensional neutron transport theory,” Nuclear Science and Engineering, 62(3), pp. 391-411 (1977).

[17] A. Rouchon, “Analyse et développement d'outils numériques déterministes et stochastiques résolvant les équations du bruit neutronique et applications aux réacteurs thermiques et rapides,” PhD thesis, Paris-Saclay University, France (2016).

[18] A. Rouchon et al., “The new 3-D multigroup diffusion neutron noise solver of APOLLO3® and a theoretical discussion of fission-modes noise,” International Conference on Mathematics & Computational Methods Applied to Nuclear Science & Engineering (M&C 2017), Jeju, Korea, April 16-20 (2017).

[19] A. Brighenti, S. Santandrea, I. Zmijarevic and Z. Stankovski, "Validation of a time-dependent deterministic model for neutron noise on the first CROCUS experimental measurements," submittted to Ann. Nuc. Energ.

[20] V. Lamirand et al., CORTEX D2.1: Experimental report of the 1st campaign at AKR-2 and CROCUS, 2018.

[21] S. Santandrea, L. Graziano, I. Zmijarevic and B. Vezzoni, "A Leakage synthetic algorithm and a Krylov approach for thermal iterations in APOLLO3 code in support to industrial applications," submitted to ANS M&C 2021 Conference.

[22] A. Brighenti, S. Santandrea, I. Zmijarevic and Z. Stankovski, "Interpretation of COLIBRI measurements in the CROCUS research reactor using a point-kinetics reactor model," the PHYTRA5 conference, 2021.

[23] A. Gammicchia, S. Santandrea, I. Zmijarevic, R. Sanchez, Z. Stankovski, S. Dulla and P. Mosca, "A MOC-based neutron kinetics model for noise analysis," Ann. Nucl. Energy, vol. 137, 2019.

[24] A. F. Henry, Nuclear-Reactor Analysis, Cambridge (MA): The MIT Press, 1986.

[25] S. Dulla, E. H. Mund and P. Ravetto, "The quasi-static method revisited," Prog. Nucl. Energ., vol. 50, no. 8, pp. 908-920, 2008.

[26] F. B. Hildebrand, Introduction to numerical analysis (second edition), New York: Dover Publications Inc., 1987.

[27] Vinai et al., CORTEX D2.5, 2021.

[28] C. Demazière, A. Tatidis and P. Vinai, “Monte Carlo-based dynamic calculations of stationary perturbations,” PHYSOR2020, EPJ We of Conferences 247, 21003 (2021).

[29] E. Brun, F. Damian, C.M. Diop, E. Dumonteil, F.X. Hugot, C. Jouanne, Y.K. Lee, F. Malvagi, A. Mazzolo, O. Petit, J.C. Trama, T. Visonneau, A. Zoia, “Tripoli-4®, CEA, EDF and AREVA reference Monte Carlo code,” Annals of Nuclear Energy, 82, Pages 151-160 (2015).

[30] A. Rouchon, A. Zoia and R. Sanchez, “A new Monte Carlo method for neutron noise calculations in the frequency domain,” Annals of Nuclear Energy, 102, April 2017, Pages 465-475 (2017).

[31] A. Rouchon, W. Jarrah and A. Zoia, “The new neutron noise solver of the Monte Carlo code TRIPOLI-4®,” Proceedings of Mathematical and Computational Methods Applied to Nuclear Science and Engineering (M&C 2019), Portland, OR, USA, August 25–29, 2019, pp. 332-341 (2019).

[32] A. Zoia, A. Rouchon, B. Gasse, C. Demazière, P. Vinai, “Analysis of the neutron noise induced by fuel assembly vibrations,” Annals of Nuclear Energy, 154, pp. 108061 (2021).

[33] T. Yamamoto, “Monte Carlo method with complex-valued weights for frequency domain analyses of neutron noise,” Annals of Nuclear Energy, 58, August 2013, Pages 72-79 (2013).

[34] T. Bahadir and S. Lindahl, “Studsvik's next generation nodal code SIMULATE-5”, Advances in Nuclear Fuel Management IV - ANFM 2009, Hilton Head Island, South Carolina, USA, April 12-15, 2009.

[35] A. Mylonakis, H. Yi, P. Vinai and C. Demazière, “Neutron noise simulations in a heterogeneous system: a comparison between a diffusion-based and a discrete ordinates solver,” International conference M&C 2019, Portland, OR, USA, August 25-29, 2019, pp. 439-448 (2019).

[36] C. Cavarec, J.F. Perron, D. Verwaerde, J.P. West, “Benchmark calculations of power distribution within assemblies,” NEA/NSC/DOC (94) 28 (1994).

[37] A. Mylonakis, P. Vinai and C. Demazière, “CORE SIM+: A flexible diffusion-based solver for neutron noise simulations,” Annals of Nuclear Energy, 155, 1 June 2021, 108149.

[38] A. Vidal-Ferràndiz, A. Carreño, D. Ginestar, C. Demazière and G. Verdú, “A time and frequency domain analysis of the effect of vibrating fuel assemblies on the neutron noise,” Annals of Nuclear Energy, 137, 107076 (2020).

[39] A. Vidal-Ferràndiz, A. Carreño, D. Ginestar and G. Verdú. “Repository of FEMFFUSION program: a finite element code for nuclear reactor modelling”. https://www.femffusion.imm.upv.es (2020).

[40] P. Vinai, H. Yi, A. Mylonakis, C. Demazière, B. Gasse, A. Rouchon, A. Zoia, A. Vidal-Ferràndiz, D. Ginestar, G. Verdú, and T. Yamamoto, “Comparison of Neutron Noise Solvers Based on Numerical Benchmarks in a 2-D Simplified UOX Fuel Assembly,” accepted in The International Conference M&C-2021, Raleigh, NC, USA, October 3-7, 2021.